

# INTERNATIONAL CONFERENCE on Microwave & THz Technologies and Wireless Communications

---

## IRPhE' 2018

---

*Dedicated to the 75th Anniversary of National Academy of Sciences of RA*

## Program and Abstract Book

**Organized by:** Institute of Radiophysics and Electronics,  
National Academy of Sciences

**Sponsored by:**



INSTITUTE OF RADIOPHYSICS  
AND ELECTRONICS



State Committee of Science  
of Armenia



September 19-21, 2018

---

**Aghveran, ARMENIA**

## **IRPhE' 2018 Main Topics:**

- **Microwave devices, antennas, propagations and remote sensing**
- **THz technique, spectroscopy and applications**
- **Wireless communications and related information technologies**
- **Alternative semiconductor and dielectric materials, electronic devices**

## **Conference Chairs:**

**ArsenHakhoumian, (Dr. Sc., Ass. Member NAS RA, IRPhE, Armenia)**

**Tigran Zakaryan (Dr. CEO IRPhE, Armenia)**

## **Program Committee:**

Radik Martirosyan, (President NAS Armenia)

Arsen Hakhoumian, (IRPhE, Armenia, *Chair IRPhE'2018*)

Kiejn Lee (Sogang University, South Korea)

Sadayuki Yoshitomi (Toshiba Corporation, Japan)

Kodo Kawase (Nagoya University, Japan)

Robert Minasyan (Sidney University, Australia)

Garik Markaryan, (Lancaster University, UK)

Stepan Petrosyan (IRPhE, Armenia)

Yuri Avetisyan (YSU, Armenia)

Khachik Nerkararyan (YSU, Armenia)

## **Organizing Committee:**

Tigran Zakaryan, (IRPhE, Chair)

Arsen Hakhoumian, (IRPhE, Co-chair)

Ashkhen Yesayan, (IRPhE, Secretary)

Emil Asmaryan (IRPhE, RA)

Hayk Manukyan (VIAVI Solutions, UK)

Anahit Mnatsakanyan (IRPhE, RA)

19 September, Wednesday

09:00 -09:30 bus pick-up near the building of National Academy of Sciences in Yerevan, 24, Marshall Baghramian Ave.

11:00-13:00	<b>Registration/Accommodation</b>	
13:00-13:45	<b>LUNCH</b>	
14:00-14:10	<b>Opening of IRPhE'2018</b> <b>Prof. Arsen Hakhoumian, IRPhE'2018 Chair</b>	
<b>Microwave devices, antennas, propagations and remote sensing, (MW)</b> <b>Chairman: Prof. Arsen Hakhoumian</b>		
14.10-14:50 <b>Keynote speech</b>	<b>Robert Minasian,</b> <i>University of Sydney, Australia</i>	<b>MW-1:</b> Advances in high-speed microwave photonic signal processing
14:50-15:20 <b>Plenary speech</b>	<b>Kiejn Lee,</b> Sogang University, South Korea	<b>MW-2:</b> 3D visualization of electromagnetic fields and thermal distribution by the thermo-elastic optical indicator microscope
15:20-15:35	<u>Arsen Hakhoumian,</u> Omid Mahmoodian IRPhE, Armenia	<b>MW-3:</b> Bessel beam radial slot antenna
15:35 - 15:50	Arsen Hakhoumian, Armen Makaryan, Nubar Poghosyan, <u>Tigran Zakaryan</u> IRPhE, Armenia	<b>MW-4:</b> Estimation of phase noise impact on coherence length in FM-CW radars with voltage controlled oscillators
15:50 -16:05	<u>Torgom Yezekyan,</u> Armen Makaryan, Vahe Tadevosyan YSU, Armenia	<b>MW-5:</b> Frequency conversion in the ferromagnet at low magnetic bias fields
16:05-16:20	<b>Coffee Break</b>	
	<b>Chairman: Prof. Robert Minasian</b>	
16:20-16:35	<u>Pavel Baybakov</u> Keysight Technologies, Russia	<b>MW-6:</b> Millimeter-wave component characterization with vector network analyzer
16:35 -16:50	Nubar Poghosyan, <u>Sargis Sargsyan,</u> Tigran Zakaryan	<b>MW-7:</b> Passive V-I Sensor Based Complex Impedance Measurement System
16:50-17:05	<u>A Sargsyan,</u> Arsen Hakhoumian,	<b>MW-8:</b> 2D dielectric periodic structure for

	IRPhE, Armenia	Microwave Polarization rotator
17:05-17:20	<u>David Nersisyan</u> , Arsen Hakhoumian, Gor Mkrtchyan, Tigran Manukyan  IRPhE, Armenia	<b>MW-9:</b> Digital Beamforming for OFDM Radar
17:20-17:30	Ruben Ter-Antonyan  National Institute of Metrology, Armenia	<b>MW-10:</b> A New Reflector Antenna Having Switchable Beam width at Operating Frequency
17:30-17:40	M.V. Markosyan, V.H. Avetisyan, <u>A.K. Aharonyan</u> , R.A. Davtyan  Yerevan Telecom Institute, Armenia	<b>MW-11:</b> The microstrip phased array antenna of centimeter waves range
17:40-17:50	M.V. Markosyan, <u>V.H. Avetisyan</u> , A.K. Aharonyan, A.A. Martirosyan  Yerevan Telecom Institute, Armenia	<b>MW-12:</b> The slotted omnidirectional antenna on a circular waveguide with mode $H_{11}$
17:50-18:00	S.B. Makarov, M.V. Markosyan, <u>V.H. Avetisyan</u> , A.K. Aharonyan, H.G. Martirosyan, R.A. Davtyan  Yerevan Telecom Institute, Armenia	<b>MW-13:</b> To problem of designing of the landing radars

<b>18:00-19:00</b>	<b>Dinner</b>	
<b>19:00-20:30</b>	<b>Welcome Reception and Poster Session</b>	
<b>Poster session (P)</b>		
Arsen Babajanyan, <u>L. Odabashyan</u> , Zh. Baghdasaryan, T. Abrahamyan, N. Harutyunyan, S. Kim, J. Kim, B. Friedman, K. Lee  YSU, Armenia	<b>MW-P_1:</b> Noninvasive in-vitro monitoring of D-glucose concentration by using a microwave fractal sensor	
Arshak L. Vartanian  YSU, Armenia	<b>EL-P_2:</b> Magnetic field control of phonon-mediated decoherence of spin-based qubit in two-dimensional quantum dot embedded in a suspended slab	
<u>Anna Asatryan</u> , A. Stepanyan, Mkrtich Yeranossyan, Albert Kirakosyan, Arshak Vartanian  YSU, Armenia	<b>EL-P_3:</b> The influence of the transverse electric field on the hot electron energy loss rate via polar-optical phonons in nanowires	
<u>Lenrik Matevosyan</u> , G. Pluzyan, K. Avjyan, G. Dabaghyan  IRPhE, Armenia	<b>EL-P_4:</b> Single-layer amorphous carbon anti-reflective coatings obtained by pulsed laser deposition method	
<u>Tigran Abrahamyan</u> , R. Khachatryan, Arsen Babajanyan, Khachatur Nerkararyan  YSU, Armenia	<b>MW-P_5:</b> Sensing of silver nanoparticles in aqueous solutions by using an optical fiber probe-tip	

Gegham Gulakyan, Armen Makaryan, <u>Ruben Miroyan</u> YSU, Armenia	<b>MW-P_6:</b> Investigation of detection of electromagnetic radiation in the plasma at the constant electric field
<u>Anahit Nikoghosyan</u> , Radik Martirosyan, Arsen Hakhoumian, Armen Makaryan, Vahe Tadevosyan, G.N. Goltsman, S.V. Antipov YSU, Armenia	<b>TH-P_7:</b> Effect of attenuation on the efficiency of THz radiation generation in a nonlinear crystal integrated into a waveguide
<u>Anahit Nikoghosyan</u> , Radik Martirosyan, Arsen Hakhoumian, YSU, Armenia	<b>TH-P_8:</b> Efficient ultrashort THz pulse generation in LiNbO <sub>3</sub> , ZnTe, GaSe and DAST crystals
Stepan Martirosyan, Albert Ghulyan, <u>Narek Yezakyan</u> , Narek Mkrtchyan, Lalayan Tamara IRPhE, Armenia	<b>MW-P_9:</b> A device for measuring body bio-impedance with combined various physical affects
<u>Stepan Martirosyan</u> , Julietta Torikyan IRPhE, Armenia	<b>MW-P_10:</b> Power analog trigger Schmitt
Norayr R. Khachatryan, <u>Ruben V. Ter-Antonyan</u> National Institute of Metrology, Armenia	<b>MW-P_11:</b> On the development of a feed for a Dual-Reflector radio-telescope with a fixed Hemispherical main reflector and a movable subreflector of the Gregory type
Ruben V. Ter-Antonyan National Institute of Metrology, Armenia	<b>MW-P_12:</b> Simple Formulae a united character simplifying the radiophysical design of Dual-Reflector Axisymmetric Antennas with a given polar equation of the generatrix of the main reflector

**20 September, Thursday**

**09:00 bus pick-up for new arrivals at the building of National Academy of Sciences in Yerevan, 24, Marshall Baghramian Ave.**

**08:00-11:00 breakfast will be served at Arturs resort canteen.**

<b>THz technique, spectroscopy and applications, (TH)</b>		
<b>Chairman: Prof. Yuri Avetisyan</b>		
09:15-09:45 <b>Plenary speech</b>	<b>Gabor Almasi</b> Institute of Physics, University of Pécs, Hungary	<b>TH-1:</b> Generation and applications of extremely high-field near single cycle terahertz pulses
09:45-10:15 <b>Plenary speech</b>	<b>Michael Bakunov</b> University of Nizhny Novgorod, Nizhny Novgorod, Russia	<b>TH-2:</b> Terahertz pulses with dc precursors
10:15-10:30	<u>Hovik Baghdasaryan</u> , T.M. Knyazyan, T.T. Hovhannisyan, A.V. Daryan, M. Marciniak National Polytechnic University of Armenia	<b>TH-3:</b> General expression of the Poynting vector operating also in the region of evanescent wave: natural quantity in the method of single expression
10:30-10:45	<u>Henrik Parsamyan</u> ,	<b>TH-4:</b> Plasmonic nanoparticles arrangements for

	Torgom Yezekyan, Hovhannes Haroyan YSU, Armenia	biosensing.
10:45-11:00	<u>Eduard Rostomyan</u> IRPhE, Armenia	<b>TH-5:</b> The dynamics of instability development in spatially separated electron beam- plasma system
11:00-11:15	<b>Coffee Break</b>	
	<b>Chairman: Prof. Gabor Almasi</b>	
11:15-11:45 <b>Plenary speech</b>	<b>Kodo Kawase</b> Nagoya University, Japan	<b>TH-6:</b> Multi wavelength is-TPG for one-shot spectroscopy
11:45-12:15 <b>Plenary speech</b>	<b>Masayoshi Tonouchi</b> Osaka University, Japan	<b>TH-7:</b> Highly sensitive THz microfluid chips coupled with a few arrays of meta-atoms
12:15-12:30	<u>Yuri Avetisyan</u> , Ruben Miroyan, Vahe Tadevosyan YSU, Armenia	<b>TH-8:</b> Noncollinear THz generation by optical rectification in periodically poled lithium niobate crystals
12:30-12:45	<u>Hovhannes Haroyan</u> , Torgom Yezekyan, Henrikh Parsamyan, Khachatur Nerkararyan YSU, Armenia	<b>TH-9:</b> Fano Resonance in coupled semicylindrical Microresonators
<b>13:00-14:00</b>	<b>LUNCH</b>	
	<b>Alternative semiconductor materials, electronic devices, (EL)</b>	
	<b>Chairman: Prof. Stepan Petrosyan</b>	
14:00-14:30 <b>Plenary speech</b>	<b>Sadayuki Yoshitomi</b> Toshiba Memory Corporation, Japan	<b>EL-1:</b> Advances of Compact Transistor Modelling Technologies for RF, millimetre-wave, and IoT Technology
14:30-15:00 <b>Plenary speech</b>	<b>Levon V. Asryan</b> Virginia Polytechnic Institute and State University, USA	<b>EL-2:</b> Close-to-ideal semiconductor lasers: Optimizing performance by suppressing recombination outside the active region
15:00-15:15	Zhyrair Gevorgian IRPhE, Armenia	<b>EL-3:</b> Quantum plateaus in dynamical Hall conductivity
15:15-15:30	Ashkhen Yesayan IRPhE, Armenia	<b>EL-4:</b> Compact transcapacitance model for short-channel FinFETs
15:30-15:45	Levon Hovakimian IRPhE, Armenia	<b>EL-5:</b> On a validity criterion for the Born approximation
15:45-16:00	<b>Coffee Break</b>	
16:00-16:15	Stepan Petrosyan, Narek Yeranyan, <u>Ashot Musayelyan</u> , Sveta Pashayan IRPhE, Armenia	<b>EL-6:</b> Characterization of CZTS thin films synthesized by two-stage magnetron sputtering on Mo covered perlite glass-crystalline substrate

16:15-16:30	Stepan Petrosyan, <u>Ashot Khachatryan</u> IRPhE, Armenia	<b>EL-7:</b> Electrical characteristics of Sb-n-InSb. Schottky barrier diodes
16:30-16:45	Stepan Petrosyan, Lenrik Matevosyan, <u>Karapet Avjyan</u> IRPhE, Armenia	<b>EL-8:</b> Charge transport mechanism in p-InSb/n-CdTe heterostructure
<b>19:30</b>	<b>Gala Dinner</b>	

**21 September, Friday**

**08:00-10:00 breakfast will be served at Arturs resort canteen.**

<b>Wireless communications and related information technologies, (WL)</b>		
<b>Chairman: Dr. Tigran Zakaryan</b>		
10:00-10:30 <b>Plenary speech</b>	<b>Hayk Manukyan</b> VIAVI Solutions, UK	<b>WL-1:</b> A Novel CoAP NB-IoT Testing Solution for 5G Wireless Networks Validation
10:30-11:00 <b>Plenary speech</b>	<b>Dmitry Titov</b> Keysight Technologies, Russia	<b>WL-2:</b> Advanced modulation and coding challenges on the way to 400G and terabit Ethernet
11:00-11:15	<u>Hovhannes Haroyan</u> , G. Hovsepyan, S. Sargsyan YSU, Armenia	<b>WL-3:</b> Power Domain Non-orthogonal Multiple Access (PD-NOMA) technique for 5G networks
11:15-11:30	<u>Gor Mkrtchyan</u> , Arsen Hakhoumian, David Nersisyan, T. Manukyan IRPhE, Armenia	<b>WL-4:</b> OFDM Radar Signal Processing
11:30-11:45	<b>Coffee Break</b>	
11:45-12:15 <b>Plenary speech</b>	<b>Faris Muhammad</b> VIAVI Solutions, UK	<b>WL-5:</b> Novel Approach to Wireless Communications Software Development Performance and Productivity Evaluation – SAFe based
12:15-12:30	<u>Muhammad Johal</u> , G. Markarian Universiti Teknikal Malaysia Melaka, Malaysia.	<b>WL-6:</b> Content-Aware Cross Layer Optimization for IMT-Advanced Systems
12:30-12:45	<u>Juwita Sultan</u> , G. Markarian, D. Zvikhachevskiy Universiti Teknikal Malaysia Melaka, Malaysia.	<b>WL-7:</b> Hybrid WiFi, WiMAX and LTE Network based on Quality of Service (QoS) using Opnet
12:45-13:00	<b>Closing Ceremony</b>	
13:00-14:00	<b>Lunch</b>	
14:00-17:00	<b>Sightseeing tour on the way back to Yerevan</b>	

**Microwave devices, antennas, propagations and  
remote sensing, (MW)**

**Session Chairs:**

**Arsen Hakhoumian, *IRPhE***

**Robert Minasian, *University of Sydney***

## **Advances in high-speed microwave photonic signal processing**

Keynote Paper

R. A. Minasian, *Fellow, IEEE, Fellow, OSA*

*School of Electrical and Information Engineering,  
University of Sydney, NSW, Sydney, 2006, Australia*

Microwave photonics offers the prospect of overcoming a range of challenging problems in the processing of signals. Its intrinsic advantages of high time-bandwidth product and immunity to electromagnetic interference (EMI) have led to diverse applications in the microwave and sensing fields. Photonic signal processing leverages the advantages of the optical domain to benefit from the wide bandwidth, low loss, and natural EMI immunity that photonics offers. Recently there has been a strong drive to realise photonic integrated circuits using Silicon Photonics. This is particularly attractive because it enables a CMOS-compatible fabrication that enables the integration of combined photonic and electronic functions on one chip. It also makes possible a cost-effective implementation with reduced footprint, power and weight. Recent advances in integrated microwave photonic signal processing and sensing are presented. These include optical single sideband modulators that can remove the effects of dispersion in wideband microwave photonic links, optical vector network analysers with high resolution, broadband tunable filters, multi-function processors, and integrated photonic sensors using optical micro-ring resonators that demonstrate extremely high sensitivity. These microwave photonic processors provide new capabilities for the realisation of high-performance signal processing and sensing.

## 3D visualization of electromagnetic fields and thermal distribution by the thermo-elastic optical indicator microscope

K. Lee<sup>1</sup>, Zh. Baghdasaryan<sup>1,2</sup>, L. Odabashyan<sup>1,2</sup>, A. Babajanyan<sup>2</sup>, S. Kim<sup>1</sup>, J. Kim<sup>1</sup>, Gerard Berthiau<sup>3</sup>, B. Friedman<sup>4</sup>

<sup>1</sup>Department of Physics & Basic Science Institute for Cell Damage Control, Sogang University, Seoul 121-742, Korea

<sup>2</sup>Department of Radiophysics, Yerevan State University, A. Manoogian 1, Yerevan 0025, Armenia

<sup>3</sup>IREENA, 44602 Saint-Nazaire Cedex, France

<sup>4</sup>Department of Physics, Sam Houston State University, Huntsville, Texas 77341, USA

We developed the 3D visualization technique - thermo-elastic optical indicator microscope (TEOIM) to map the electromagnetic near-field and thermal distributions caused by the DC and AC influences. Additionally, we performed 3D visualization at a fixed frequency which well-illustrated the near-field distribution changes in space. COMSOL Multiphysics simulation has been done in order to understand heating principles and spatial distribution origin. Experimental results were in good agreement with simulations data.

To illustrate the practicality of the technique for the defects measurement we visualized the near-field distribution on FM antenna PCB. Obtained images well describe the field distribution changes in defect located areas and the defects influence on the overall antenna geometry as well.

To characterize the losses of an anisotropic composite material were characterized due to the microwave radiation influence we take the advantages of TEOIM technique. 3D visualization showed that the near-field distribution stretches along the composite material high conductivity axis and takes different forms when some defects in the composite material were analyzed.

This technique may give significant information to engineers for designing and optimizing patterned circuits and microstrips. Due to its high sensitivity, it can successfully apply in a wide range of testing and defects discovering applications.

### Acknowledgments

This work was supported by Basic Science Research Program through the National Research Foundation of Korea (NRF) funded by the Ministry of Education (2018R1D1A1B07047984, 2015R1D1A1A02061824, and 2009-0093822).

## **Bessel beam radial slot antenna**

O.Mahmoodian, A.Hakhoumian

*Institute of Radiophysics and Electronics, Alikhanian Brothers str . 1.0203 Ashtarak, Armenia*

The resonance type radial slot antenna as a high efficiency Bessel beam launcher was designed and investigated in wide band of operation frequencies. The analytical method to determine resonant frequencies of short-circuit radial line was evaluated and applied to calculation of the resonant frequencies of the radial resonators with different modes number, dielectric permittivity and sizes. The experimental results are in good agreement with calculation once. The expression for  $E$  and  $H$  are obtained and applied to the calculation of both electric and magnetic fields distributions. The impedance, voltage and current of radial line are investigated and related diagrams of intended modes are plotted. The circular slots are located on the top plate of radial line and are excited by the radially inward traveling transverse electromagnetic (TEM) mode in the upper part of line. The slots are arrayed on top plate which they can couple with the radial current flowing over the line to produce a radially polarized broadside beam. The position of these radiating slots is estimated from the maximum values of current distribution of line. The far field radiation pattern of radial slot antenna is measured and plotted for different distances. It was founded that the observe at the distance up to  $70\lambda$ .

## Estimation of Phase Noise Impact on Coherence Length in FM-CW Radars with Voltage Controlled Oscillators

A.A. Hakhoumian, A.H. Makaryan, N.G. Poghosyan, T.V. Zakaryan\*

*Institute of Radiophysics and Electronics, Armenian National Academy of Sciences  
Alikhanian 1, Ashtarak, 0203, Armenia*

\*E-mail: tigr@irphe.am

In this paper we analyze phase noise “propagation” within FM-CW radar originated from voltage controlled oscillator (VCO), which is of great importance from the viewpoint of effective moving target indication (MTI).

Let's start from the spectrum of frequency noise  $L_0^\omega(\omega)$  of VCO, which is like cut white noise. The coherence length is defined as the width of equi-area rectangular having the height equal to the maximum value of correlation function. Taking into account the well-known relation between spectra of frequency and phase noises (stationary case), as well as Wiener-Khinchin theorem, finally we find for coherence length the following estimation

$$\tau_{coh} = \frac{1}{2\pi t_0^2 L_0^\omega},$$

where  $t_0$  is round-trip time delay to the target, and  $L_0^\omega$  is spectral density of frequency noise of VCO. Obviously, better oscillators and less time delays result in longer coherence length.

### References

- [1]. M. Skolnik, Introduction to Radar Systems, 3rd ed. (McGraw-Hill, New York, 2001)
- [2]. V. Carotenuto *et al.*, IEEE Radar Conf., Arlington VA, 10-15 May (2015), 0274.
- [3]. A. Hakhoumian *et al.*, Electromagnetic Waves and Electronic Systems **16** (2011) 43 (in Russian).

## Frequency conversion in the ferromagnet at low magnetic bias fields

T. Yezekyan, A. Makaryan, V. Tadevosyan

*Radiophysics and Electronics Dept., Yerevan State University, Yerevan, Alex Manoogyan str. 1, 0203 0025 Armenia*

The detection and second harmonic generation of microwave radiation in a ferromagnetic material at low magnetic bias fields was experimentally obtained at room temperature.

Low-frequency ferrites of different grades and sizes were used as ferromagnetic samples. The microwave signal was fed to ferromagnetic samples by means of inductive coils wound around the samples. The entire system was placed in an external adjustable magnetic field.

On certain conditions, under the influence of the microwave signal, the magnetic moment of the magnetized ferrite performs nonlinear oscillations, as a result of which the frequency conversion occurs. For the registration of aforementioned converted signal various coil inductors wound around ferromagnetic sample were used.

The dependence of the converted signal on the magnetizing field was measured for different forms of the magnetization curve. It was shown that the conversion efficiency depends strongly on the shape of the magnetization curve of the ferromagnetic sample, as well as on the magnitude of the magnetizing field. Particularly, the quadratic nonlinear phenomena is not observed without an external magnetized field.

The results of this study may find applications for the registration and frequency conversion of radiation, for information data recording and so on.

## Millimeter-wave component characterization with vector network analyzer

P. Baybakov

*Keysight Technologies, Moscow, Russia*

### I. INTRODUCTION

In a world of interconnection, the need to transmit more information faster is driving designers to millimeter-wave (mmwave) frequencies, 30 to 300 GHz. This range is named for the 1 mm to 10 mm wavelengths at these frequencies. Microwaves can carry up to about 1 Gbit/s, but millimeter waves offer transmission rates of 10 Gbit/s or higher.

The most prominent applications of mmwave technology are 5G, WiGig, automotive radar, aerospace and defense industry. All of these applications present unique challenges in their testing and application. Error sources such as cable losses, connector repeatability, and phase shifts that might have been mostly negligible at radio frequencies are amplified at higher frequencies. High-end vector network analyzers typically have maximum frequencies of 67 GHz, so many of these applications require testing beyond the limits of most hardware. However, there are now ways to increase the frequency range of VNAs.

### II. SOLUTION

The N5291A measurement solution for mmwave network analysis is a distributed system composed of a vector network analyzer (VNA), a test set controller, and frequency extenders. A distributed system is made up of separate components that communicate together to act as one system. The frequency extenders interface with the device under test (DUT) and are the only pieces of the system that operate at mmwave



*Figure 1—N5291A mmwave measurement system*

frequencies.

This allows us to test mmwave devices without having to completely rebuild VNAs to handle higher frequencies. The frequency extenders connect to a test set controller, which interfaces with the test set of the VNA. This gives the VNA a new maximum frequency of 120 GHz so it can test modern mmwave devices.

The key advantages are:

1. Single sweep, traceable measurements with minimum measurement uncertainty from 900 Hz to 120 GHz due to standardized 1 mm coaxial connector.
2. Typical dynamic range >110 dB up to 110 GHz, >100 dB up to 120 GHz.
3. Temperature stability due to separate frequency extension modules with convection cooling.

### III. REFERENCES

- [1] Keysight Technologies, “How can distributed architecture help mmwave network analysis?”, white paper, May 2018
- [2] Keysight Technologies, “Achieving metrology-grade results at millimeter-wave frequencies”, application note, June 2018

## Passive V-I Sensor Based Complex Impedance Measurement System

N.G. Poghosyan, S.T. Sargsyan, T.V. Zakaryan

*Institute of Radiophysics and Electronics, Armenian National Academy of Sciences  
Alikhanian 1, Ashtarak 0203, Armenia*

Nowadays in modern semiconductor manufacturing processes the using of dry etching has many advantages over the standard wet one [1]. For dry semiconductor etching they use the plasma generated from high power radio frequency (RF) signal. From technological point of view, plasma generated from the RF power should meet several requirements. The most important one is homogeneous and constant plasma density. The homogeneousness of the plasma in the chamber is achieved in the development stage [2]. Meanwhile, the constant plasma density depends on the RF signal constant energy flow to the chamber. It is not a trivial problem because the generated plasma impedance changes nonlinearly and should be tracked in order to match generator with the plasma. Plasma impedance precise measurement allows to achieve this goal. To put it in another way, the power delivered to the plasma chamber, namely the plasma density, will be constant. It should be mentioned that during the plasma material processing the plasma parameters' nonlinear changing causes the high order harmonics growing at RF generator and plasma section. In this respect, the high order harmonics should be tracked as well to know process stage in the plasma chamber.

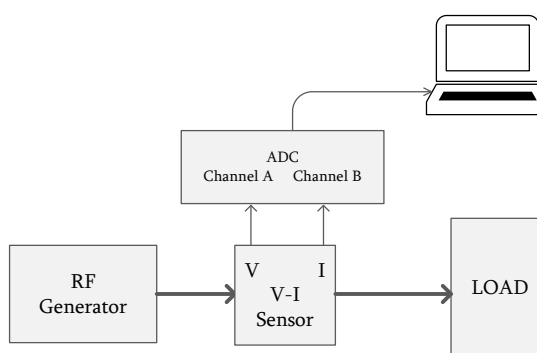


*Fig. 1 A direct digital impedance measurement device block diagram*

General setup of the plasma impedance measurement is shown in Fig.1: voltage-current (V-I) sensor has been placed between the RF generator and plasma chamber, V-I sensor [3] has two outputs shown the “voltage” and “current” proportional signals of RF flow thought. Thereupon these two signals are used to measure the impedance of the plasma.

In this article the direct digital method for impedance measurement is introduced (see Fig.1). The accuracy of the phase measurement is estimated. Initial system calibration technique is presented and several known load impedances are measured.

**Conclusion.** The method of measurement of RF impedance is proposed based on direct digitalization of VI sensor signals. The accuracy of this method versus sampling frequency is estimated and testing results for several known loads are presented.

### References

1. Grill A., “Cold Plasma in Material Fabrication, From Fundamental to Applications”, New York: IEEE Press, 1994, 257.
2. Gavrilov N.V, Emlin D.R., Nikulin S.R. “Generation of a homogeneous plasma in a glow discharge with a hollow anode and a wide-aperture hollow cathode” Technical Physics Letters, June 1999, Volume 25, Issue 6, pp 498–500
3. Агаджанян А.А., Ахумян А.А., Закарян Т.В., Меликян А.К., Погосян Н.Г., Саргсян С.Т., “Методы мониторинга и управления радиочастотной плазмы в современных технологических процессах”, физические основы приборостроения, 2016, Т5-№1(18), стр. 78-87

## 2D dielectric periodic structure for microwave polarization rotator

Armen Sargsyan<sup>1</sup>, Arsen Hakhoumian<sup>2</sup>

<sup>1</sup>Yerevan State University, Yerevan, Alex Manoogyan str. 1, 0203 0025 Armenia

<sup>2</sup>Institute of Radiophysics and Electronics, Armenian National Academy of Sciences  
Alikhanian 1, Ashtarak 0203, Armenia

The periodic dielectric structures related to the wide class of the photonic crystals (PC) having grate potential for application in various purpose microwave devices. The fabrication process of a dielectric PC is compatible with 3D printed technology which allows to realizing the all dielectric hybrid microwave integrated circuits. One of the critical elements of the PC based integrated microwave circuits is the polarization rotator. Our goal is study and design of such devices on base of anisotropy dielectric permittivity of 2D dielectric periodic structures. The structures was prepared from synthetic cordierite ( $2MgO2Al_2O_35SiO_2$ ), dielectric permittivity  $\varepsilon = 4,7$ .

The elementary sell is a square hole with inner size  $a = 1mm$  and dielectric wall  $t = 0,2mm$ . The polarization phenomena was investigated at Ku band where wavelength is  $\lambda \gg a$  those no photonic band gap phenomena can be occur.

On base of this 2D structure the high efficiently polarization rotators was designed and tested. The typical length of rotators is  $L \approx 6\lambda$  and polarization conversion efficiency more than 95%. The linear to circular polarization converter was designed as well.

## Digital Beamforming for OFDM Radar

D. Nersisyan,<sup>1,2</sup> A. Hakhumyan<sup>1</sup>, G. Mkrtchyan<sup>1,2</sup>, T. Manukyan<sup>1,2</sup>

<sup>1</sup>*Institute of Radiophysics and Electronics, Alikhanian Brothers str. 1, 0203 Ashtarak, Armenia*

<sup>2</sup>*YEA Engineering, Engineering City, Bagrevand 21/1, Nor Nork, 0062 Yerevan Armenia*

This work presents the design of a transmitter and receiver for the 3D OFDM RADAR. Receiver's part consists of 4 antennas and each of that has 5 rectangular patch elements. The type of feeding for these antennas is serial. To achieve better side lobe level the rectangular patch sizes modified by the Dolph-Chebyshev function. Transmitter consists of one antenna with the same characteristics and size, which is receiver's. The receiver antenna array beam-width in azimuth plane is 25° and in elevation plane is 60°.

Digital Beamformer (DBF) based on the mathematical model of a far-field plane wave incident on a antenna array. Simulations of a DBF transmitter and receiver are performed to control the power pattern of a 4-element linear array. An implementation of a DBF receiver was performed using a digital processing board containing a Xilinx Kintex-7 410T FPGA to control the radiation pattern of a Phased Array antenna. There used the parallel signal processing which allows to scan all sector simultaneously. For this application used the 8 beams which quantity is scalable. The quantity of beams depends on FPGA resource. By using DBF the 3 modes have been developed: Normal (Figure 1), Offset (Figure 2), Mono (Figure 3).

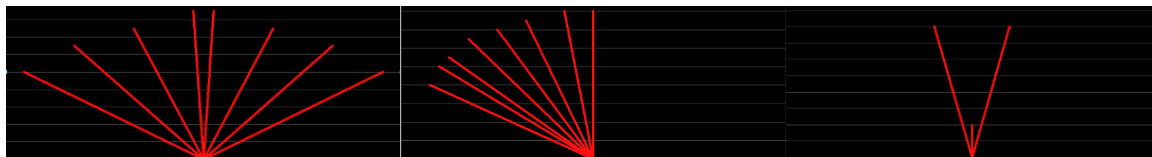


Figure 1

Figure 2

Figure 3

The applications of this modes are different. The Normal mode uses for the scanning the area to detect the targets. In the offset mode all beams concentrated on the smaller sector which gives more angle resolution. In the Mono mode beams maximum and minimum levels are mostly expressed which gives the opportunity to track the target.

## **A New Reflector Antenna Having Switchable Beamwidth at Operating Frequency**

Ruben V. Ter-Antonyan

*National Institute of Metrology, Komitas Ave., 49/3, Yerevan, Armenia*

A dual-reflector axisymmetric antenna with a mechanical beamwidth switching(expansion or narrowing) is proposed, characterized in that the expansion(narrowing) of beam is accompanied by not a quadratic and an almost proportional decrease(increase) of the antenna gain.

The antenna consists of a spherical main reflector, a two-way subreflector with significantly different geometries of the sides, which is able to rotate about an axis perpendicular the axis of symmetry of the antenna and intersecting this axis, with an axisymmetric fixation of one side or the other facing the main reflector, and a horn feed located on the axis of symmetry between main reflector and subreflector. The formulae which are necessary for radiophysical design of the antenna, and calculations confirming proportionality are given.

## The microstrip phased array antenna of centimeter waves range

M.V. Markosyan<sup>1,2</sup>, V.H. Avetisyan<sup>1,2</sup>, A.K. Aharonyan<sup>1,2</sup>, R.A. Davtyan<sup>1</sup>

<sup>1</sup> *Yerevan Telecommunication Institute, Dzorapi str. 26, 0015 Yerevan, Armenia*

<sup>2</sup> *Russian-Armenian University, H. Emin str. 123, 0051 Yerevan, Armenia*

[mark@yeti.am](mailto:mark@yeti.am), [aharaharonyan@gmail.com](mailto:aharaharonyan@gmail.com)

In this paper a module of linear array antenna for a circular view with a single excitation point is proposed. With his module the structure of the phased array working in the range 8.9-9.1 GHz and consisting of 16 sub arrays was designed. The that design of the phased array allows to reduce the number of receiver and transceiver modules of the system, since one module provides the operation functionality of 16 transmitting and receiving elements. This makes it possible to simplify the lattice design, which leads to a reduction in the cost of the system. Such flat antenna arrays are used in survey terrestrial radars, in onboard radars with a synthetic aperture for monitoring the earth's surface.

## The slotted omnidirectional antenna on a circular waveguide with mode $H_{11}$

M.V. Markosyan<sup>1,2</sup>, V.H. Avetisyan<sup>1,2</sup>, A.K. Aharonyan<sup>1,2</sup>, A.A. Martirosyan<sup>2</sup>

<sup>1</sup> Yerevan Telecommunication Institute, Dzorapi str. 26, 0015 Yerevan, Armenia

<sup>2</sup> Russian-Armenian University, H. Emin str. 123, 0051 Yerevan, Armenia

[mark@yetri.am](mailto:mark@yetri.am), [avahan@mail.ru](mailto:avahan@mail.ru)

The investigation results of unusual paired slotted radiating structures of a circular waveguide with the main  $H_{11}$  mode are discussed. The designing of those structures are based on known polarization degeneration phenomenon of wave with this mode. In the waveguide cross-section, the centers of the half-wave transverse paired slots are spaced by an angle  $\gamma$  over both sides of the waveguide diametric line along the polarization direction of the  $H_{11}$  mode. The radiation patterns at different spaced angles  $\gamma$  as well as at the two-tier location of such paired slots are investigated. The second tier is located along the waveguide longitudinal axis on the distance equals to half of the waveguide wavelength. The paired slots of those tiers have the same spaced  $\gamma$  angle, but they are located at the opposite sides of the waveguide. The omni-directional slotted antenna is offered which is designing on a combination of the two-tiered structure with opposite frontal slots and the two two-tier structures with opposite paired slots. The unevenness of the radiation pattern of designing antenna does not exceed 3 dB.

## To problem of designing of the landing radars

S.B. Makarov<sup>1</sup>, M.V. Markosyan<sup>2,3</sup>, V.H. Avetisyan<sup>2,3</sup>, A.K. Aharonyan<sup>2,3</sup>,  
H.G. Martirosyan<sup>2</sup>, R.A. Davtyan<sup>2</sup>

<sup>1</sup> *St. Petersburg Polytechnic University, Polytechnicheskaya str. 29, 195251 Saint Petersburg, Russia*

<sup>2</sup> *Yerevan Telecommunication Institute, Dzorapi str. 26, 0015 Yerevan, Armenia*

<sup>3</sup> *Russian-Armenian University, H. Emin str. 123, 0051 Yerevan, Armenia*

[mark@yetri.am](mailto:mark@yetri.am), [avahan@mail.ru](mailto:avahan@mail.ru)

Two structural diagrams for the designing of landing radars that meet modern requirements for airport traffic capacity and reliability of aircraft landing are compared. The first diagram of radar construction is based on the use of a single receiving-transmitting phased array antenna that forms a scanning four-beam directional pattern. The second diagram is the radar with separated receiving and transmitting antenna systems. The phased array antenna is also used as the receiving antenna system. A separate transmitting antenna system consists of a set of separate radiating units, each of which sequentially irradiates its section of the radar coverage area by switching of the transmitter to a choosing unit. The process of searching of an aircraft and measuring its angular coordinates, range and speed in a particular area section of the radar coverage is synchronized with the switching of the microwave probing transmitter signal to the unit irradiating this section. Possible circuits of microwave switches are presented. Some characteristics of both radars are discussed with a view to evaluating the possibility of their implementation.

## Noninvasive in-vitro monitoring of D-glucose concentration by using a microwave fractal sensor

A. Babajanyan<sup>1</sup>, L. Odabashyan<sup>1,2</sup>, Zh. Baghdasaryan<sup>2</sup>, T. Abrahamyan<sup>1</sup>, N. Harutyunyan<sup>3</sup>,  
S. Kim<sup>2</sup>, J. Kim<sup>2</sup>, B. Friedman<sup>4</sup>, K. Lee<sup>2</sup>

<sup>1</sup>Department of Radiophysics, Yerevan State University, A. Manoogian 1, Yerevan 0025, Armenia

<sup>2</sup>Department of Physics & Basic Science Institute for Cell Damage Control, Sogang University, Seoul 121-742, Korea

<sup>3</sup>Qaghsi Secondary School SNO, Kotayk, Armenia

<sup>4</sup>Department of Physics, Sam Houston State University, Huntsville, Texas 77341, USA

Microwave fractal sensor (MFS) was used for noninvasive in-vitro monitoring of the D-glucose concentration in the range of 0-0.25 range at about 6 GHz operating frequency. Sensor based on modified first fractal order Hilbert curve design and measured D-glucose concentrations in aqueous solutions by using a real-time microwave near-field electromagnetic interaction technique. We observed  $S_{11}$  reflection parameters (which depend on the glucose concentration in solution) of the fractal sensor at resonant frequencies. The measured minimum detectable signal was 0.0178 dB/(mg/dl) and the measured minimum detectable concentration was 1.68 mg/dl. The in-vitro results show the measured signal-to-noise ratio of about 28dB. This proposed system provides a unique approach for real-time in-vitro biological monitoring and control.

### Acknowledgments

This work was supported by Basic Science Research Program through the National Research Foundation of Korea(NRF) funded by the Ministry of Education (2018R1D1A1B07047984, 2015R1D1A1A02061824, and 2009-0093822).

## **Sensing of silver nanoparticles in aqueous solutions by using an optical fiber probe-tip**

T.Abrahamyan<sup>1</sup>, R.Khachatryan<sup>2</sup>, A. Babajanyan<sup>1</sup>, Kh. Nerkararyan<sup>1</sup>

<sup>1</sup>*Department of Radiophysics, Yerevan State University, A. Manoogian 1, Yerevan 0025, Armenia*

<sup>2</sup>*Microwave Systems & Measurements Lab, Institute of Radiophysics & Electronics at NAS RA, Alikhanian 1, Ashtarak 0203, Armenia*

In this paper we investigate the properties of silver nanoparticles in distilled water by using the resonance of surface plasmon-polaritons (SPPs) with the gold-coated optical fiber probe-tip. The observed SPP intensity at resonance was changed depending on silver nanoparticles concentration in the aqueous solution due to the change in of the permittivity of the solution. This method allowsto create a new chemical sensor to monitoring metal particles concentration in liquids.

## **Investigation of detection of electromagnetic radiation in the plasma at the constant electric field**

G. Gulakyan<sup>1</sup>, A. Makaryan<sup>2</sup>, R. Miroyan<sup>2</sup>

<sup>1</sup>*Information Systems Service and Development Departmet, YSU Ijevan Branch, Ijevan, Usanoghakan str. 3, 4001  
Armenia*

<sup>2</sup>*Radiophysics and Electroniks Dept., Yerevan State University, Yerevan, Alex Manoogyan str. 1, 0203 0025  
Armenia*

The investigation results of the detection of electromagnetic radiation in a glow discharge plasma of various gases in present work we report.

The different types of neon and xenon gas-discharge lamps were used as detectors. The voltage to the lamp was applied from a current source, providing a glow discharge in the lamp. It was shown that the detection efficiency depends strongly on the shape of the I-V characteristic of a gas-discharge lamp, as well as on the applied voltage (electric field).

The dependence of the detection efficiency on the polarization of electromagnetic radiation was investigated.

The detection of a pulsed neodymium laser in air at an external electric field was also investigated. A constant voltage, close to the breakdown threshold of air ( $\sim 2000$  kV / m), was applied to the parallel electrodes through the ballast resistor.

Under the joint action of the laser pulse and the applied electric field, in the focusing region of the laser beam breakdown of air occurs. Thanks to the constant applied field, the created plasma behaves as a medium with a quadratic nonlinearity, which makes it possible to detection of electromagnetic radiation.

## **A device for measuring body bioimpedance with combined various physical affects**

A. Martirosyan Stepan<sup>1</sup>, B. Ghulyan Albert<sup>1</sup>, C. Yezakyan Narek<sup>1</sup>, D. Mkrtchyan Narek<sup>2</sup>, E. Lalayan Tamara<sup>2</sup>

<sup>1</sup> *Institute of Radiophysics and Electronics, Alikhanian Brothers str. 1, 0203 Ashtarak, Armenia*

<sup>2</sup> *Izmirlyan Medical Center, Aharonyan str. 6, 0069 Yerevan, Armenia*

In the article is described a biomedical device which is foreseen for use diagnostically and investigator purposes in biomedical tissues and skin, body's different parts. It is made first prototype of the device.

In the person the doctor can externally affect different types of biocurrents (i.e. direct, alternate, pulse and so on). In the past many doctors and scientists do very much researches and experiments in human body. So after the procedure it can be easily detected if the patient has an illness and what is the patient's diagnostic.

Several medical procedures can be done by using the device: electro sleep, diadinamotherapia, electro analgesia, galvanization and so on.

The device measures bioimpedance of the person suspended by temperature in the different points of the skin. The affecting direction of active points can be changed.

The software will be provided in the second version. By using the computer it is foreseen to save medical data and to do long time investigations for every patient.

## **Power analog trigger Schmitt**

Martirosyan Stepan<sup>1</sup>, Torikyan Julietta<sup>1</sup>

<sup>1</sup> *Institute of Radiophysics and Electronics, Alikhanian Brothers str. 1, 0203 Ashtarak, Armenia*

Our designed electrical appliance is intended for use in managing and controlling devices as a powerful electrical coupling hub. It is a functional equivalent of the HEF4093 integrated circuit and is assembled on the basis of a modern integrated circuit (comparator) and a MOSFET transistor for power output. The input of the scheme require digital or analog signal. At the output of the device possible to switch the load which may have high currents. If the output current is higher than the specified (selective) value, the scheme automatically switches to a generation mode. It allows current load's mean value limitation within the permitted current of the MOSFET transistor used. The transistor is even protected from the short load mode due to the control duty cycle of output pulses ( $Q = T / t \geq 1$ ). The scheme's structure allows the free choice of comparator and transistor based on the required electrical parameters.

The device model has been tested on 1-15 amperes range.

## **On the Development of a Feed for a Dual-Reflector Radio Telescope with a Fixed Hemispherical Main Reflector and a Movable Subreflector of the Gregory Type**

Norayr R. Khachatryan, Ruben V. Ter-Antonyan

*National Institute of Metrology, Komitas Ave., 49/3, Yerevan, Armenia*

It is emphasized that when the location of the subreflector vertex is chosen very close to the paraxial focus in order to reduce its overall dimensions and, accordingly, the weight, the amplitude distribution the in-phase field in the movable aperture of the radio telescopes (RT) in the transmit mode is an inversion of the feed pattern, which makes it unacceptable to use widespread types of feeds with a cosinusoidal pattern as not providing an acceptable value of the gain factor of the RT. It is proposed to compensate the inverse action of the subreflector by successive modification of the shape of the feed pattern using the algorithmic procedure for maximizing the gain factor, which is represented as a ratio of two quadratic forms. For example, for the ROT - 32/54/2.6 the results of numerical experiments on the development of feed patterns, which successively equalize the amplitude distribution of the field in the aperture, increasing the gain factor from 0.82 to 0.93, is presented.

## **Simple Formulae a United Character Simplifying the Radiophysical Design of Dual-Reflector Axisymmetric Antennas with a Given Polar Equation of the Generatrix of the Main Reflector**

Ruben V. Ter-Antonyan

*National Institute of Metrology, Komitas Ave., 49/3, Erevan, Armenia*

For dual-reflector axisymmetric antennas with a given polar the equation the generatrix of the main reflector, including those displaced relative the axis rotation, the simplest way is to obtain the polar parametric equations for a plane curve, the segments of which can serve as generatrix of subreflectors ensuring, as a minimum, the point focus. As the current parameter selected polar angle the generatrix main reflector, what made the equations are a source of comprehensive information about optical scheme every possible of dual-reflector axisymmetric antennas, in particular, antennas with a parabolic, spherobolic, Schwarzschild, circular, rectilinear generatrix of the main reflector. Also the explicit expression for the transforming function is given which, by multiplying by the radiation pattern of the feed, transfer the latter into the inphase distribution of the field in the antenna aperture. The formulae specified in the examples of parabolic and circular generatrix of the main reflector.

# **THz technique, spectroscopy and applications, (TH)**

**Session Chairs:**

**Yuri Avetisyan, *Yerevan State University***

**Gabor Almasi, *University of Pécs***

## Generation and applications of extremely high-field near single cycle terahertz pulses

G. Almási<sup>1</sup>, Z. Tibai<sup>1</sup>, G. Krizsán<sup>1,2</sup>, B. Kovács<sup>1</sup>, P.S. Nugraha<sup>1,2</sup>, L. Tokodi<sup>1</sup>, L. Pálfalvi<sup>1</sup>, J.A. Fülöp<sup>2,3</sup>, J. Hebling<sup>1,2,3</sup>

<sup>1</sup>*Institute of Physics, University of Pécs, Ifjúság St. 6, 7624 Pécs, Hungary*

<sup>2</sup>*Szentágotthai Research Centre, University of Pécs, Ifjúság St. 20, 7624 Pécs, Hungary*

<sup>3</sup>*MTA-PTE High-Field Terahertz Research Group, University of Pécs, Ifjúság St. 6, 7624 Pécs, Hungary*

In the last twenty years the energy of near-single-cycle terahertz pulses increased by many orders of magnitude from the femtoJoule to the milliJoule level [1, 2]. Extremely high (field strength exceeding 10 MV/cm) terahertz electric fields are offering now good application possibilities for electron acceleration [3,4] and charged particle beam manipulation [5]. The needs to increase the energy and peak electric field strength of THz pulses requires the continual development of terahertz sources. Optical rectification of ultrashort optical pulses in nonlinear crystals is the most successful method for near-single-cycle terahertz pulse generation. LiNbO<sub>3</sub> is an excellent material for terahertz generation due to its exceptionally high value of its  $d_{33}$  second order nonlinear optical tensor element. However the phase matching of the pump and generated pulses which is necessary for the efficient generation can be a challenge, if the refractive indices in the optical and terahertz range differ significantly. For such cases the tilted-pulse-front (TPF) geometry [6] is the exclusive solution for the necessary phase matching. In the conventional TPF setup the pulse front tilting is done by a diffraction grating and some imaging optics. Unfortunately, this setup is not freely scalable due to some limitations of the setup. Imaging errors can be avoided by the application of the contact grating setup but due to the wedge shape of the nonlinear material it is hard to produce large terahertz beams with good focusability. In the presentation two different setups will be proposed eliminating the error sources of the above mentioned solutions. Hybrid scheme [7] will be analyzed where the pulse front tilting is realized in two steps. Another possible solution will be introduced as well where a stair-step echelon produces the tilt [8] and in that case slab shaped crystal can be used eliminating distortion caused by the prism shape nonlinear material.

In the second part of the talk the results of numerical simulations of electron acceleration will be presented where electrons from rest will be accelerated up to a few hundred of keVs by the application of two, milliJoule level single-cycle terahertz pulses. The acceleration is realized in three stages. In the first stage two counter propagating single-cycle terahertz pulses having the same waveform and polarization direction create a transient standing wave. This field will accelerate the electrons which are produced by a synchronized short pulse laser focused into a gas jet. The generated electrons are then accelerated by the superposition of the two terahertz pulses. In the second stage also two (or four) counter-propagating terahertz beams will interact with the electron bunch. In this case half of the terahertz beams are retarded by LiNbO<sub>3</sub> plates in order to eliminate the decelerating effect of the terahertz beam. In the third accelerating stage a terahertz driven dielectric structure will be used for the post acceleration of the electron bunch. Advantages of the terahertz wavelength will be shown compared to dielectric laser accelerators driven by optical waves.

### References:

- [1] J. A. Fülöp et al., Opt. Expr. 22, 20155 (2014),
- [2] C. Vicario C et al., Opt. Lett. 39, 6632 (2014),
- [3] E.A. Nanni et al., Nat. Commun. 6, 8486 (2015),
- [4] W.R. Huang et al., Sci. Rep. 5, 14899 (2015)
- [5] J. Hebling et al., arXiv:1109.6852 (2011)
- [6] J. Hebling et al., Opt. Expr. 10, 1161 (2002)
- [7] L. Pálfalvi et al., Opt. Expr. 24, 8156 (2016)
- [8] L. Pálfalvi et al

## Terahertz pulses with dc precursors

M. I. Bakunov<sup>1</sup>, E. S. Efimenko<sup>2</sup>, M. V. Tsarev<sup>3</sup>, and S. A. Sychugin<sup>1</sup>

<sup>1</sup> University of Nizhny Novgorod, Nizhny Novgorod, Russia

<sup>2</sup> Institute of Applied Physics, Russian Academy of Sciences, Nizhny Novgorod, Russia

<sup>3</sup> Ludwig-Maximilians-Universität München, Garching, Germany

Optical rectification of high-intense ultrashort laser pulses in electro-optic crystals has emerged as the most efficient method for generating strong electric and magnetic fields in the terahertz frequency range. The demand for stronger terahertz fields requires increasing the laser pump intensity. At high pump intensities, multiphoton absorption becomes a significant factor that can limit the generation efficiency. Multiphoton absorption leads not only to the pump depletion but also to the creation of free carriers that absorb terahertz radiation. Thus, free-carrier generation is commonly considered as a detrimental effect for terahertz generation.

Recently, it was found that free carrier generation can give rise to a new physical effect, namely, the generation of quasistatic electromagnetic fields propagating ahead of the laser pulse, i.e., a dc precursor [1]. The mechanism of the effect is related to the nonstationarity of the optically ionized crystal. The newly created carriers are accelerated by the electric field that copropagates the rectified laser pulse. The acceleration produces a surge of an electric current, which in turn generates the precursor. The predictions of Ref. [1] were based on a one-dimensional model and the assumption of undepleted pump. Here we explore the effects of laser beam focusing and pump depletion on the precursor generation. To circumvent the negative effect of depletion, we propose to use chirped laser pulses as a pump. We also demonstrate that using the tilted-pulse-front pumping technique [2] allows one to increase the generated precursor fields by orders of magnitude.

Figure 1(a) shows snapshots of the electric field  $E_y$  generated by a Ti:sapphire laser pulse (780 nm wavelength) propagating along the  $z$  axis in a 3-mm thick GaP crystal.  $E_y$  is normalized to the amplitude of the nonlinear polarization  $P_0$  induced by the laser pulse in the crystal. If pump depletion is neglected, the precursor has a form of a plateau, whose size increases with distance in the crystal and due to transmission through the crystal boundary. Pump depletion leads to an attenuation of the rear part of the precursor.

For negatively chirped laser pulse, dispersive compression of the laser pulse in the crystal [Fig. 1(c)] sustains high optical intensity [Fig. 1(b)] and, therefore, efficient precursor generation. The precursor's shape is almost completely restored due to chirped-pulse pumping [Fig. 1(a)].

To extend the precursor generation to highly nonlinear crystals, such as LiNbO<sub>3</sub>, we propose to use tilted-pulse-front laser pulses [2]. For example, a pulse with a 1.05  $\mu\text{m}$  wavelength, 64.5° tilt angle, 300 fs duration, and 70 GW/cm<sup>2</sup> peak intensity can generate in a 5 mm long crystal a 1 mm long precursor with a 250 kV/cm electric field.

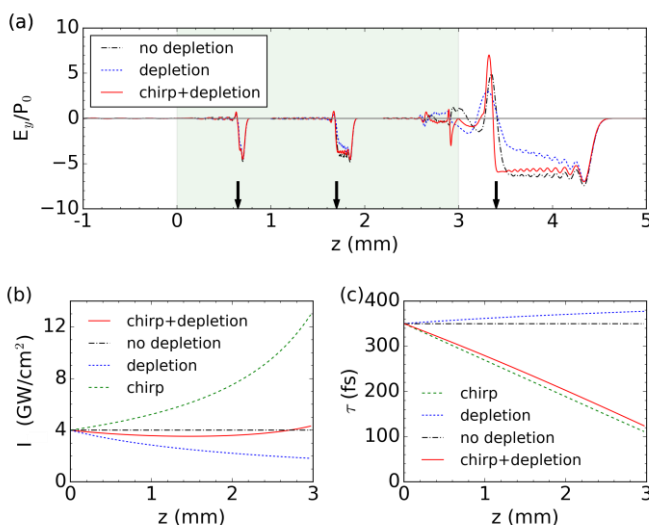


**Fig. 1.** (a) Snapshots of  $E_y/P_0$  at three moments of time for the cases when pump depletion is neglected, included, and compensated by chirping the laser pulse. The crystal (shaded region) is 3 mm thick. The arrows depict the position of the pump pulse. (b) Intensity and (c) duration of the pump pulse as a function of the distance in the crystal.

1. M.I. Bakunov, A.V. Maslov, and M.V. Tsarev, *Phys. Rev. A* **95**, 063817 (2017).

2. J. Hebling, G. Almasi, I.Z. Kozma, and J. Kuhl, *Opt. Express* **10**, 1161 (2002).

## General expression of the Poynting vector operating also in the region of evanescent wave: natural quantity in the method of single expression

H.V. Baghdasaryan<sup>1</sup>, T.M. Knyazyan<sup>1</sup>, T.T. Hovhannisyan<sup>1</sup>,  
A.V. Daryan<sup>2</sup>, M. Marciniak<sup>3</sup>

<sup>1</sup>National Polytechnic University of Armenia, 105 Terian str., Yerevan 0009, Armenia

Tel: +374 99 11 05 47, e-mail: [hovik@seua.am](mailto:hovik@seua.am)

<sup>2</sup>A.Alikhanyan National Laboratory, Cosmic Ray Division, 2 Alikhanyan brothers str., Yerevan 0036, Armenia

<sup>3</sup>National Institute of Telecommunications, 1 Szachowa Street, 04-894 Warsaw, Poland

In unbounded region of evanescent waves, where electric and magnetic fields are diminishing values, the traditional Poynting vector becomes purely imaginary indicating impossibility of electromagnetic energy transfer [1]. However, a confined region of evanescent wave permits transferring energy through it, e.g. transmission through a piece of undersized waveguide, energy transmission at frustrated total internal reflection, etc. In quantum mechanics, where time-independent Schrödinger equation is similar to the Helmholtz's equation, the tunneling, i.e. transmission through a potential barrier is observed [2]. In confined regions of evanescent waves the traditional expression for the Poynting vector is useless as evanescent waves are inhomogeneous waves. Traditional methods of boundary problems solution operate with the Poynting vector only outside of the evanescent waves region [3]. In opposite, in the method of single expression (MSE) [4-6], in any boundary problem solution the Poynting vector is calculated also within the media under analysis. In the MSE, where an assumption of counter-propagating waves is not used, the general expression for the Poynting vector at any point of a medium is an integrable quantity and expressed as:

$$P_z(z) = \frac{c^2}{8\pi\omega} U^2(z) \frac{dS(z)}{dz},$$

where  $U(z)$  and  $S(z)$  are real values describing resultant amplitude and phase of an electromagnetic wave in a medium. Outside of the region of evanescent waves full agreement with the Poynting vector in a traditional form is obtained. The general expression of the Poynting vector permits to monitor energy transfer process within any confined wavelength-scale evanescent wave region that is topical for a correct design of nano-optical devices. The relevant expression for the probability flow density valid within the potential barrier in quantum mechanics has been obtained recently [7].

### REFERENCES

- [1] J.A. Stratton: *Electromagnetic Theory*, McGraw – Hill Book Company, Inc., (1941).
- [2] S.V. Gaponenko, *Introduction to Nanophotonics*, Cambridge University Press (2010).
- [3] F. de Fornel: *Evanescent Waves from Newtonian Optics to Atomic Optics*, Springer, (1997).
- [4] H.V. Baghdasaryan, “Method of backward calculation”, in the book: “Photonic Devices for Telecommunications: how to model and measure”/ Editor G. Guekos, Springer-Verlag, (1999), pp.56-65.
- [5] H.V. Baghdasaryan, T.M. Knyazyan, “Problem of Plane EM Wave Self-action in Multilayer Structure: an Exact Solution”, *Optical and Quantum Electronics*, **31** 1059 (1999).
- [6] H.V. Baghdasaryan, T.M. Knyazyan, T.H. Baghdasaryan, B. Witzigmann, and F. Roemer, “Absorption loss influence on optical characteristics of multilayer distributed Bragg reflector: wavelength-scale analysis by the method of single expression”, *Opto–Electronics Review*, vol. 18, Issue 4, pp. 438–445, (2010).
- [7] H.V. Baghdasaryan, T.M. Knyazyan, T.T. Hovhannisyan, M. Marciniak, “Solution of Boundary Problems in Intensity-Dependent Nano-Optics and Quantum Mechanics by the Method of Single Expression”, *Proceedings of ICTON 2017 Conference*, 2-6 July 2017, Girona, Spain, Tu.B4.3, 7 pages. (2017).

## Plasmonic Nanoparticles Arrangements for Biosensing.

H. Parsamyan<sup>1</sup>, T. Yezekyan<sup>1</sup>, H. Haroyan<sup>1</sup>.

<sup>1</sup> Yerevan State University, Alex Manoogian str. 1, 0025 Yerevan, Armenia

The need for a fast, ultracompact, highly-sensitive, label-free and reliable devices for biosensing has provided a growing interest [1]. Localized surface plasmon resonance (LSPR) has emerged as a leader among label-free biosensing techniques offering sensitive, robust, and facile detection [2]. The sensing principle relies on LSPR spectral shifts caused by the change of surrounding dielectric environment during a binding process.

The use of noble metal nanoparticles in biosensing has grown enormously in recent years, mainly due to several advantages over other traditional biosensing methods. Since the nanoparticles themselves are colored, detection can often be carried out with the naked eye, yielding rapid, portable detection. In addition, the production and fabrication of nanoparticles, which contain small amounts of material, is often inexpensive.

However, several challenges still remain which limit the use of noble metal nanoparticles in various biosensing applications. This work is focused on improvement of LSPR biosensors by using different geometries and arrangements of nanoparticles. Here we present the numerical analysis of the LSPR of the single gold (Au) and silver (Ag) nanoparticles (NP) of spherical and cubic shapes, and for different spatial arrangements (such as dimers) as well. To have a LSPR in visible region, the diameter of the spheres and the sides of the cubes were chosen 50 nm. Comparative analyses of the extinction cross section ECS (both absorption and scattering cross sections) of the single cubic and spherical NPs (see Fig.1. (a)), as well as for cube-cube and sphere-sphere NP dimers were carried out.

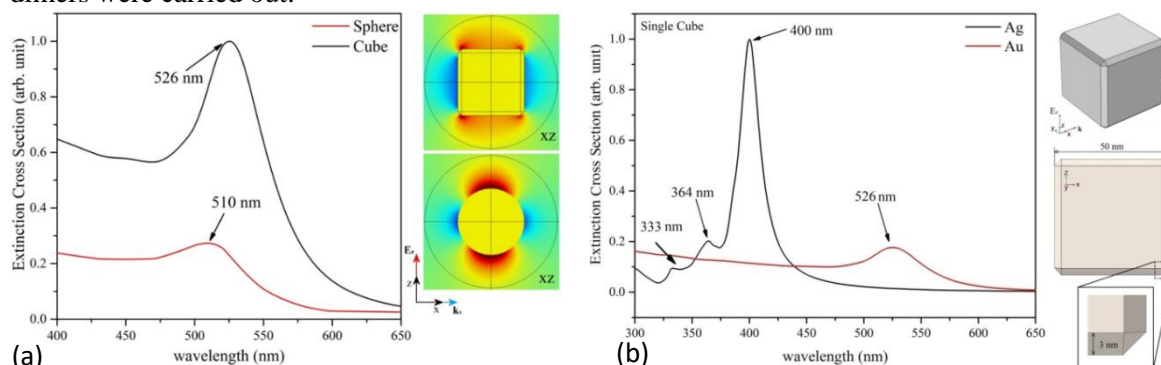


Fig.1. (a) Extinction Cross Sections of gold (Au) sphere and cube nanoparticles vs. incident field wavelength, (b) Extinction Cross Sections of gold (Au) and silver (Ag) nanocubes vs. incident field wavelength.

Study of the dependence of the LSPR of the cubic NP on the different values of chamfering radius (0-ideal cube, 3nm and 5 nm) shows the red shift of the resonance with decreasing the chamfering radius. For the silver nanocube the analysis shows three extinction peaks: on  $\sim 333$  nm,  $\sim 364$  nm due to strong absorption and on  $\sim 400$  nm due to scattering, whereas for gold nanocube only one extinction peak exists on  $\sim 526$  nm (see Fig.1(b)). Obtained results show that silver nanocubes and dimmers have the advanced capabilities compared to gold nanospheres with same dimensions. For instance ECS of single silver nanocube is higher up to 25 times compared to gold nanosphere.

### References

1. Unser, S., Bruzas, I., He, J., & Sagle, L. Localized surface plasmon resonance biosensing: current challenges and approaches. *Sensors* 15.7 (2015): 15684-15716.
2. Chen, S., Svedendahl, M., Käll, M., Gunnarsson, L., & Dmitriev, A. Ultrahigh sensitivity made simple: nanoplasmonic label-free biosensing with an extremely low limit-of-detection for bacterial and cancer diagnostics. *Nanotechnology* 20.43 (2009): 434015.

## The dynamics of instability development in spatially separated electron beam- plasma system

E.V.Rostomyan

*Institute of Radiophysics and Electronics, Alikhanian Brothers str. 1, 0203 Ashtarak, Armenia )*

Plasma filled microwave devices (amplifiers and generators) have many advantages as compared to well-known vacuum devices [1-2]. Modern devices correspond to cylindrical waveguide with thin annular plasma and spatially separated thin annular electron beam [1-2]. Operation of these sources is based on the beam interaction with the surface wave of hollow plasma cylinder and instability development. Present investigation considers detailed properties of the instability in system consisting of electron beam and spatially separated dissipative plasma. A study is developed that allows carrying out the investigation in general form, independently on system geometry, specific parameters etc. It only is assumed slight overlapped of the beam and the plasma fields (so called weak beam-plasma coupling). In this case the beam-plasma interaction significantly differs from conventional case of full overlap (strong coupling). Under weak coupling proper oscillations of the beam reveal themselves efficiently and the instability is caused by excitation of negative energy beam wave (NEBW). Developed approach is based on representation of growing fields in form of wave train with slowly varying amplitude (SVA) and transformation of the dispersion relation to an equation for SVA. Its solution actually presents results of important problem of time evolution of initial perturbation. Obtained analytical expression by itself gives detailed information on the instability, most of which is unavailable by other methods. The analysis is visible and gives incomparably more detailed results than conventional initial/boundary problems. The solution also obviously shows that with increase in level of dissipation the instability caused by NEBW growth gradually transforms to a new, up to recently unknown type of dissipative streaming instability. Its growth rate has more critical, than conventional, inverse proportional dependence on dissipation. Presented approach allows tracing the detailed properties of any streaming instability [3-4].

- [1] M. V. Kuzelev A. A. Rukhadze Plasma Phys Report v. 26, p.231, 2000
- [2] M. V. Kuzelev, O. T. Loza, A. A. Rukhadze, P. S. Strelkov, and A. G. Shkvarunets Plasma Phys Report v.27, p.669, (2001).
- [3] E.V.Rostomyan. *The behavior of streaming instabilities in dissipative plasma*. Lambert Academic publishing ISBN 978-3-569-89294-3, 2018.
- [4] E.V.Rostomyan. in *Plasma Science. Basic fundamentals and Modern Applications*. InTechOpen Publ Group. 2018

## Multi wavelength is-TPG for one-shot spectroscopy

K. Murate, Y. Guo, K. Maeda, and K. Kawase

<sup>1</sup> Nagoya University, Furocho, Nagoya, Japan

For several years, we have worked on the development of an injection-seeded terahertz (THz) parametric generator (is-TPG) as a high-power THz-wave source. Recently, the peak output power of is-TPG approached a few tens of kW after introducing a microchip Nd:YAG laser with a shorter pulse width. However, long measurement times are necessary for spectroscopic imaging because is-TPG is a tunable source that emits a single wavelength in each pulse. We recently generated multiwavelength THz waves from is-TPG. In multiwavelength generation, the wavelength does not need to be tuned, allowing a spectrum to be acquired in a single pulse. Therefore, the measurement time can be drastically shortened by using this system for spectroscopic imaging. Furthermore, we introduced a new scheme that improved the stability by acquiring reference spectrum at the same time.

When a high-power pump beam and seed beam imping on a LiNbO<sub>3</sub> crystal, a narrow line width and high brightness THz wave is generated by parametric wavelength conversion [1]. Wide tunability of the is-TPG can be achieved by controlling the wavelength of the seed beam and its angle to satisfy the non-collinear phase-matching condition of the LiNbO<sub>3</sub> crystal. In this study, we generated multiwavelength THz waves by injecting multiwavelength seed beams into the crystal and distributing the energy to each wavelength[2]. For the multiwavelength seed beams, we used multiple external cavity laser diodes (ECLDs) with semiconductor optical amplifier.

Figure 1 shows the experimental setup for the high-speed and stabilized THz spectroscopic imaging system. The emitted multiwavelength THz waves were split into two beams to obtain not only a sample measurement beam but also a reference beam simultaneously. After passing through a sample, the sample measurement beam was focused onto the crystal for detection. The reference beam was directly input to another detection crystal. Finally, the THz waves were detected based on nonlinear optical wavelength conversion [1], whereas the infrared (IR) detection beam intensities were measured using an IR beam profiler. The detection beams were angle-dispersive, allowing each wavelength to be detected separately. The simultaneous acquisition of the reference and detection beams improved measurement stability.

Next, we report the one-shot spectroscopic measurement of three saccharides using this system. We placed pellets with 40% maltose, glucose, and lactose in the THz-wave optical path and recorded the spectroscopic measurements. We confirmed that the attenuation of the THz waves matched the absorption spectra of the reagent, and qualitatively identified the saccharides using one-shot multi-wavelength is-TPG with good output stability. The measurement can be performed at a frame rate equal to the laser's repetition, enabling real-time reagent identification.

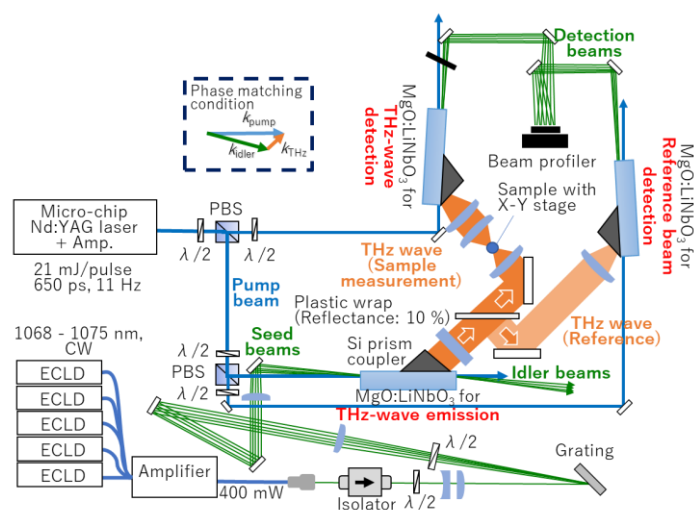


Fig. 1. Experimental setup of high-speed terahertz (THz) spectroscopic imaging system using multiwavelength injection-seeded THz parametric generator (is-TPG).

The authors appreciate the fruitful discussions with Dr. S. Hayashi of NICT; Dr. H. Minamide and Dr. K. Nawata of Riken; and Prof. T. Taira of IMS. This work was partially supported by JSPS KAKENHI Grant Number 18H03887.

- [1] S. Hayashi, K. Nawata, T. Taira, J. Shikata, K. Kawase, and H. Minamide, *Sci. Rep.*, 4 (2014) 5045.
- [2] K. Murate, S. Hayashi, and K. Kawase, *Appl. Phys. Express* 10 (2017) 032401.
- [3] K. Kawase, Y. Ogawa, Y. Watanabe, and H. Inoue, *Opt. Express* 11(2003) 2549.
- [4] M. Kato, S. R. Tripathi, K. Murate, K. Imayama, and K. Kawase, *Opt. Express* 24 (2016).

# Highly sensitive THz microfluidic chips coupled with a few arrays of meta-atoms

Masayoshi Tonouchi

*Institute of Laser Engineering, Osaka University, 2-6 Yamadaoka, Suita, 565-0871, Japan*

**Abstract:** We developed a terahertz microfluidic chip with a few arrays of split ring resonators. The obtained resonance spectrum shows the high-sensitive frequency shift to detect femtomol of solutes in sub nanoliter of solution.

## 1. Introduction

Microfluidic devices are well known as one of the promising analytical systems for medical diagnosis and chemical analysis due to their potentials to be reduced sample volumes, low cost and etc.[1]. On the other hand, the advantageous properties of bio-sensing with terahertz (THz) waves, such as possibilities of detecting the molecular vibration and rotation in a label-free fashion, are also receiving a lot of attentions in various fields[2]. Application of microfluidics to THz technology will attract attention not only for the development of compact THz bio sensors but also for the possibility to build new analytical THz devices. However, it is challenging for measuring ultra-trace solution with THz waves due to the spatial resolution of far-field THz waves and the strong absorption into polar solvent. To overcome these problems, we have shown that the locally generated intense-THz wave source by laser irradiation is effective for high-sensitive THz spectroscopy and imaging of minute substances of subwavelength scale as well as ultra-trace solution[3-5]. Here, we take advantage of this technique to develop a THz microfluidic chip and demonstrated THz time-domain spectroscopy of trace amount of solution.

## 2. Experimental

Figure 1 shows a schematic drawing of the concept of the THz microfluidic chip. Here we employed a nonlinear optical crystal, GaAs, as a THz emitter. The chip consists of a single microchannel, 11x11 arrays of split ring resonators and a point THz radiation source that is generated in the process of optical rectification in the GaAs on a sub-wavelength scale. The solution flowing into the microchannel with its actual volumes of 318 picoliter modify the resonance frequency in the THz transmission spectra.

## 3. Results

Figure 2 shows a plot of the resonance frequency shift ( $\Delta f_R$ ) of mineral water with different hardness (10mg/L, 40mg/L and 200mg/L) as a function of the mole number. Here,  $\Delta f_R \equiv |f_R - f_0|$ , where  $f_R$  and  $f_0$  are the observed resonance frequency of the mineral water and pure water (0mg/L), respectively. All the samples were repeatedly measured 10 times for reliability and the error bar of each sample was derived from maximum and minimum values. It is found that the minute change of the minerals of ~10 mg/L was sensitively detected. This sensitivity corresponds to 31.8 femtomol according to the calculation using volume of the microchannel and the molar mass of the minerals[6]. As a result, we showed that the fabricated THz-chip can be worked as a high-sensitive sensor for measuring ultra-trace solution and could be contributed for micro analytical technology in biological and medical fields.

This work was partially supported by JSPS KAKENHI Grant Numbers JP15K18053 and JP17H01269.

[1] J. Castillo-León, and W. E. Svendsen ed., Springer, 2014.

[2] M. Tonouchi, "Cutting-edge terahertz technology," *Nat. Photonics* **1**, 97 (2007).

[3] K. Serita et al., "Scanning laser terahertz near-field imaging system," *Opt. Express* **20**, 12959 (2012).

[4] H. Murakami et al., "Scanning laser terahertz imaging system," *J. Phys. D: Appl. Phys.* **47**, 374007 (2014).

[5] K. Serita et al., "Direct measurements of terahertz meta-atoms with near-field emission of terahertz waves," *J. Infrared Milli. Terahz. Waves* **38**, 1107 (2017).

[6] K. Serita et al., "Terahertz microfluidic chips sensitivity-enhanced with a few arrays of meta-atoms," *APL Photonics* **3**, 051603 (2018).

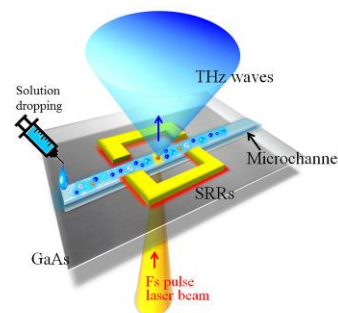


Fig.1. A schematic drawing of THz microfluidic chip

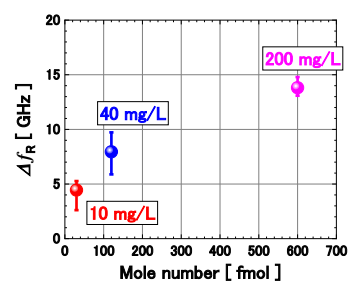


Fig.2. Resonance frequency shift as a function of the mole number of mineral water.

## **Noncollinear THz generation by optical rectification in periodically poled lithium niobate crystals**

Y. Avetisyan, R. Miroyan, V. Tadevosyan

*Microwave Radiophysics Dept., Yerevan State University, Alex Manoogian str. 1, 0025 Yerevan, Armenia*

The method of terahertz (THz) generation by optical rectification of the femtosecond laser pulses in the periodically poled lithium niobate (PPLN) crystal has attracted much interest due to its simplicity and relatively high generation efficiency. Although in PPLN crystals narrowband THz waves are generated in various directions (with different central frequencies), they were mainly observed in directions either parallel or perpendicular to the propagation direction of the laser pulses.

In present report, the angular-frequency distribution of THz wave generation in common 1-D and slant-stripe PPLN structures are analyzed. In the latter case the precise control of the phase-matching condition allows generating narrowband THz-waves with high efficiency, especially if PPLN crystal is pumped by intensity modulated laser radiation (at the designed frequency of generation) and cryogenically cooled to reduce the THz absorption inside the material. In the former case we show that placing a dielectric THz grating (with a period equal to spatial period of the PPLN structure) on the lateral surface of the PPLN crystal results in formation of nearly single-cycle (broadband) THz radiation.

## Fano Resonance in Coupled Semicylindrical Microresonators

H. Haroyan<sup>1</sup>, T. Yezekyan<sup>1</sup>, H. Parsamyan<sup>1</sup>, Kh. Nerkarayan.

<sup>1</sup> Yerevan State University, Alex Manoogian str. 1, 0025 Yerevan, Armenia

Efficient and low-loss optical coupling to high quality (Q) factor Whispering Gallery Mode (WGM) microresonators is important for a wide range of applications include frequency and soliton mode-locked microcombs, bio and nano-particle sensors [1,2].

Recent developments have greatly improved the sensitivity of optical sensors based on metal nanoparticle arrays and single nanoparticles. This kind of sensors is used for biosensing purposes that is to detect molecular binding events and changes in molecular conformation. The device is based on biological, or bioinspired receptor unit with unique specificities toward corresponding analytes. These analytes are often of biological origin like DNAs of bacteria or viruses, or proteins which are generated from the immune system (antibodies, antigens) of infected or contaminated living organisms. Still, one of many other challenges in biosensor development is the sensitivity.

On the other hand, since its discovery, the asymmetric Fano resonance has been a characteristic feature of interacting quantum systems. Recently, the Fano resonance has been found in plasmonic nanoparticles, photonic crystals, and electromagnetic metamaterials and there are several papers on the use of that effect for biosensors.

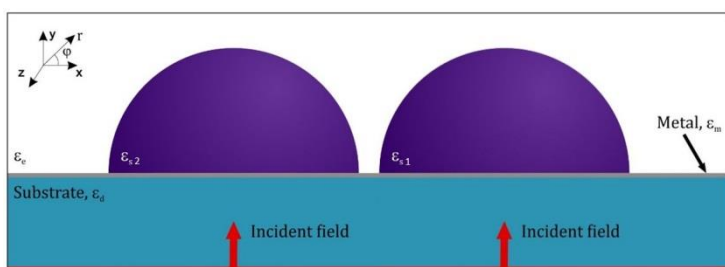


Fig. 1. The cross section of the structure of semicylindrical microresonator.  $\epsilon_s = 2.25$ ,  $\epsilon_e = 1$  are dielectric permittivities of the substrate (SiO<sub>2</sub> Silica) and the surrounding medium (Air), respectively. As a metal and semicylinder medium Ag and GaAs ( $\epsilon_{s1}$ ) and Si (Silicon- $\epsilon_{s2}$ ) were used correspondingly.

Proposed structure consists of two coupled semicylinders with different mediums placed on metal thin layer; an incident plane wave is used to excite resonators (see Fig.1). The main advantage of this structure is in the easy coupling method with incident plane wave. Resonator system combines properties of Fabry-Perot resonator, where the input of wave energy is carried through mirrors, and cylindrical resonator, where Whispering-gallery modes with azimuthal  $m$  and radial  $\ell$  mode numbers are formed. Here, the possibility of simple input and output of radiation is combined with the possibility of using the unique properties of an evanescent wave on cylindrical surface of a dielectric. The control of evanescence coupling between two resonators is realized by varying the distance between resonators. By changing the angle of incidence the wave vector in the plane perpendicular to semicylinder axes, we change the phase shift between the exciting waves of two different resonators, hence tuning the system under the conditions of Fano resonance.

### References

1. K. J. Vahala, "Optical microcavities," *Nature* **424**, 839–846 (2003).
2. F. Vollmer and L. Yang, "Label-free detection with high-Q microcavities: a review of biosensing mechanisms for integrated devices," *Nanophotonics* **1**, (2012).
3. H. Haroyan, H. Parsamyan, T. Yezekyan, Kh. Nerkararyan, *Applied Optics* **57**, 6309-6313 (2018).

## Effect of attenuation on the efficiency of THz radiation generation in a nonlinear crystal integrated into a waveguide

A.S. Nikoghosyan<sup>1</sup>, R.M. Martirosyan<sup>1</sup>, A.A. Hakhoumian<sup>2</sup>, A.O. Makaryan<sup>1</sup>,  
V.R. Tadevosyan<sup>1</sup>, G.N. Goltsman<sup>3</sup>, S.V. Antipov<sup>3</sup>

<sup>1</sup> Yerevan State University, Alex Manoogian str. 1, 0025 Yerevan, Armenia

<sup>2</sup> Institute of Radiophysics and Electronics, Alikhanian Brothers str. 1, 0203 Ashtarak, Armenia

<sup>3</sup> Moscow State Pedagogical University, Moscow, 119571, Russia

The effect of THz radiation absorption on the efficiency of generation of coherent THz radiation in a nonlinear optical crystal integrated into a metal rectangular waveguide is studied. The generation of the THz pulse is based on the mixing of the spectral components of a femtosecond optical laser pulse in a nonlinear crystal (optical rectification method). The efficiency of the nonlinear conversion of optical laser radiation to the THz band is also a function of the phase-matching (PM) condition inside the nonlinear crystal, that is to say of the equality of the group velocity of the optical pulse and of the phase velocity of the THz pulse at the difference frequency. The method of partial filling of a metal waveguide with a nonlinear optical crystal is used to ensure phase matching. Phase matching was obtained by the proper choice of the thickness of the nonlinear crystal, namely the degree of partial filling of the cross section of the waveguide.

We have studied the THz radiation damping caused by the losses in both the metal walls of the waveguide and in the crystal, taking into account the dimensions of the cross section of the waveguide, the thickness of the crystal (the degree of partial filling) and its dielectric constant.

DAST, LiNbO<sub>3</sub> and ZnTe crystals were studied due to the high efficiency of conversion of optical radiation to THz in them. On the other hand, such crystals demonstrate effective second order nonlinear susceptibility and have various dielectric constants for which the PM condition is satisfied.

It is shown that the attenuation of THz pulses increases with the degree of filling of the given cross-section of a waveguide. However, in the case of a small dielectric permittivity and partial filling, the losses in the metal walls are comparable to the losses in the walls of an unfilled metal waveguide. In addition, in the case of a thin crystal with a low dielectric permittivity, attenuation can be weaker than in an unfilled waveguide. In a partially filled waveguide, this phenomenon occurs because of the decrease of the cut-off frequency, which is more obvious when the waveguide is completely filled with a crystal. In the case of a high dielectric permittivity of the crystal, the losses in the walls of the waveguide are observed to be higher, which is more due to the degree of filling with the crystal than due to the frequency. In all crystals, a minimum attenuation is observed for a certain frequency band.

## Efficient ultrashort THz pulse generation in LiNbO<sub>3</sub>, ZnTe, GaSe and DAST crystals

A.S. Nikoghosyan<sup>1</sup>, R.M. Martirosyan<sup>1,2</sup> A.A. Akhumyan<sup>3</sup>.

<sup>1</sup> Yerevan State University, Alex Manoogian str. 1, 0025 Yerevan, Armenia

<sup>2</sup> National Academy of Sciences of the Republic of Armenia, 24/5, Marshall Baghramian Ave., 0019 Yerevan, Republic of Armenia

<sup>3</sup> Institute of Radiophysics and Electronics, Alikhanian Brothers str. 1, 0203 Ashtarak, Armenia

Due to the achievements of nonlinear optics, in particular nonlinear frequency conversion of femtosecond optical laser pulses in the terahertz (THz) range and the development of THz sources and detectors, interest in effective waveguide systems has grown considerably. The value of the generated terahertz power limits the major specifications of the THz coherent techniques in imaging and tomography.

Among nonorganic nonlinear crystals the semiconductor crystals GaAs, InTe, ZnTe, GaP, possess a high nonlinear coefficient  $d_{14}$  of the order 100 pm/V or more, and among organic crystals DAST and DANPH have the same property. Since these semiconductor crystals are nonbirefringent, they cannot be phase matched by angle tuning.

The calculated data as well as the results of the effective generation of terahertz (THz) radiation in the band 0.1-2.5 THz via optical rectification of femtosecond laser pulses in LiNbO<sub>3</sub>, ZnTe, DAST, GaSe nonlinear optical crystals, partially filling the cross section of the rectangular waveguide are presented. The phase matching of a nonlinear polarization wave and the difference frequency radiation (DFR) can be achieved by choosing the crystal filling degree of a rectangular waveguide. In this case the crystal acts both as a nonlinear frequency converter and a GHz-THz wave phase velocity moderator.

Any non-linear optical crystals with selected high non-linear second-order susceptibility, having low absorption coefficients and low dispersion, may also be used as antenna for ultra-high-speed electronic integrated circuits.

The results can be used for creating effective THz broadband active waveguide system or frequency scanning antenna.

**Alternative semiconductor materials, electronic  
devices, (EL)**

**Session Chair:**

**Stepan Petrosyan, *IRPhE***

# Advances of Compact Transistor Modelling Technologies for RF, millimetre-wave, and IoT Technology

Sadayuki Yoshitomi

Design Technology Innovation Division  
TOSHIBA Memory CORPORATION  
2-5-1, Kasama Sakae-Ku, Yokohama, 247-8585, Japan

Since the 1st evolution of the CMOS single chip transceiver in late 1990s, there are outstanding developments in the field of high speed RF/millimeter wave CMOS device fabrication and circuit design technologies. Besides, measurement and precise compact modelling technologies in order to fully characterize these devices have been greatly developed. These is no doubt successful development of accurate compact model leads successful design of RF/millimeter wave ICs, which requires simulation accuracy with the aid of accurate compact models.

Author think tackling with three issues (1) overcoming millimeter wave measurement uncertainty, (2) visualize the global and local variations of devices' millimeter-wave characteristic and (3) develop its statistical model. Former requires advancement of measurement technique for obtaining stable and trustworthy measurement data, and latter require absolutely accurate compact model to predict devices' statistical distribution in the millimeter-wave frequency domain. To solve these issues, combined knowledge of RF/millimeterwave characterization technique, device fabrication and knowledge of device physics to infer the source of fluctuation is required.

commonplace of semiconductor design related technologies, which also be needed for the design of future IoT applications. In this work, I would like to show how to solve these issues. Working examples with 65 and 40 nm RF-CMOS generation nodes are shown in the presentation.

The ways to realize efficient update of compact models can be applied to efficient yield control of millimeter-wave chips' production. The keyword is the establishing link with smartfactory, which provides model users with accurate yield prediction and design infrastructure for robust circuit design. This can be realized by the access and analysis of the big-data, in which monitored devices' statistic data are stored, and by the timely development of process based millimeter-wave Monte Carlo model.

Author regard realization of such technologies and their implementation into existing circuit design flow as the new subject of compact modeling research and development field which is different from current direction of the compact modeling technology focusing on the creating mathematical formulae of semiconductor devices with new materials, new structures and ultra-small dimensional structures.

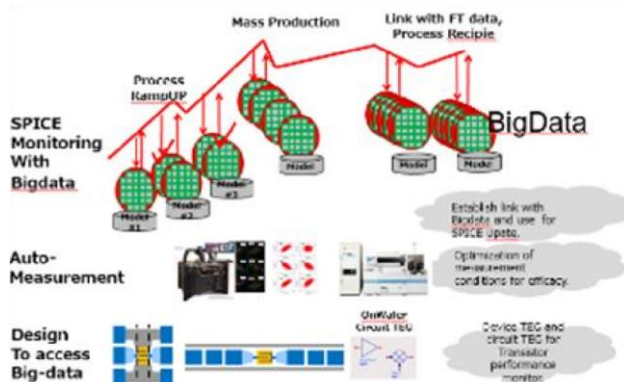


Fig. 1. Concept of compact modelling development in the future SmartFactory. By using the Bigdata coming from the production line is to update typical and sigma value of the statistical model. To establish the iteration loop will contribute the production yield. New direction of the compact modelling technology

Realization of accurate compact models in order to meet aforementioned requirements stand in the

## REFERENCES

- [1] Franz Sischka, "ICCAP Modeling Handbook", Keysight Technologies.
- [2] K. Takano, S. Amakawa, K. Katayama, et al., "Modeling of short-millimeter-wave CMOS transmission line with lossy dielectrics with specific absorption spectrum," IEICE Trans. Electron., vol. E96-C, no. 10, pp. 1311–1318, March 2013.
- [3] Seitaro Kawai, Shinji Sato, Shotaro Maki, et al., "Accurate Transistor Modeling by Threeparameter Pad Model for Millimeter-Wave CMOS Circuit Design," IEEE Transactions on Microwave Theory and Techniques, Vol. 65, No. 6, pp. 1736-1744, June 2016.
- [4] Sadayuki Yoshitomi, "Challenges to Accuracy for the Design of DeepSubmicron RF-CMOS Circuits", Mixdes Conference 2005, Poland..
- [5] Ohguro, "The impact of Oxinitride process, deuterium annealing and STI stress to 1/f noise of 0.11um CMOS", VLSI 2003, pp37-38
- [6] Sadayuki Yoshitomi, "Compact Model Challenges of 65nm RF-CMOS Technology", MOS-AK/ESSDERC/ESSCIRC Workshop, Edinburgh (2008).
- [7] Tom Lee, "CMOS LNA and Mixer Design", CICC short Course (2009).
- [8] Sadayuki Yoshitomi, "Characterization and modeling of RF-MOSFETs in the millimeter-wave frequency domain", MOS-AK meeting 2013 (Washington).

## Close-to-ideal semiconductor lasers: Optimizing performance by suppressing recombination outside the active region

Levon V. Asryan

*Virginia Polytechnic Institute and State University, Blacksburg, USA*

In conventional diode lasers with a low-dimensional active region, the electrons and holes are first injected from the cladding layers into a bulk reservoir, which also serves as the waveguiding layer [optical confinement layer (OCL)]. The carriers are then transported to the active region and, finally, captured into the latter. Due to bipolar (i.e., both electron and hole) population in the OCL, a certain fraction of the injection current goes into electron-hole recombination there. This parasitic recombination outside the active region is a major source of the temperature dependence of the threshold current [1]. In addition, the carrier capture from the OCL into the active region is not instantaneous. For this reason, the carrier density in the OCL, and hence the parasitic recombination rate, rise, even above the lasing threshold, with injection current. This leads to sublinearity of the light-current characteristic (LCC) and limits the output power, especially at high pump currents [2–4].

To suppress the recombination outside the quantum-confined active region, two design approaches were proposed. One of the approaches [5–11] exploits double tunneling-injection (DTI), i.e., tunneling injection of both electrons and holes into the active region from two separate quantum wells (QWs). In a DTI laser, the quantum-confined active region, located in the central part of the OCL, is clad on each side by a thin barrier and a QW. Electrons and holes are injected into the active region by tunneling from the corresponding QWs. Ideally, there should be no second tunneling step, i.e. out-tunneling from the active region into the ‘foreign’ QWs (electron-injecting QW for holes and hole-injecting QW for electrons).

The other approach [6, 7] is based on independent tailoring of the conduction and valence bandedges by means of the use of two asymmetric barrier layers (ABLs) – one on each side of the active region. The ABL in the electron-injecting side of the structure should ideally prevent holes from entering that side while not hindering the electron-injection into the active region. The ABL in the hole-injecting side should prevent electrons from entering that side while not hindering the hole-injection into the active region. A laser utilizing ABLs was termed a bandedge-engineered laser [6, 7, 12] or an ABL laser [13–15].

In both DTI and ABL lasers, there will be no electrons (holes) in the hole- (electron-) injecting side of the structure, i.e., the bipolar population will be suppressed outside the active region.

As discussed in this presentation, the total suppression of bipolar population and, hence, of recombination outside the active region would result in close-to-ideal operating characteristics in DTI and ABL lasers, namely, virtually temperature-insensitive threshold current, close-to-one internal quantum efficiency, and linear LCC. The dynamic characteristics would also be improved in these lasers [16, 17].

This work was supported by the US Army Research Office under Grant No. W911NF-17-1-0432.

- [1] L. V. Asryan and R. A. Suris, *Semicond. Sci. Technol.* **11**(4), 554 (1996).
- [2] L. V. Asryan, S. Luryi, and R. A. Suris, *Appl. Phys. Lett.* **81**(12), 2154 (2002).
- [3] L. V. Asryan, S. Luryi, and R. A. Suris, *IEEE J. Quantum Electron.* **39**(3), 404 (2003).
- [4] L. V. Asryan and Z. N. Sokolova, *J. Appl. Phys.* **115**(2), 023107 (2014).
- [5] L. V. Asryan and S. Luryi, *IEEE J. Quantum Electron.* **37**(7), 905 (2001).
- [6] L. V. Asryan and S. Luryi, *Solid-State Electron.* **47**(2), 205 (2003).
- [7] L. V. Asryan and S. Luryi, *U.S. Patent 6 870 178 B2*, Mar. 22, 2005.
- [8] D.-S. Han and L. V. Asryan, *Appl. Phys. Lett.* **92**(25), 251113 (2008).
- [9] D.-S. Han and L. V. Asryan, *Solid-State Electron.* **52**(10), 1674 (2008).
- [10] D.-S. Han and L. V. Asryan, *J. Lightw. Technol.* **27**(24), 5775 (2009).
- [11] D.-S. Han and L. V. Asryan, *Nanotechnology* **21**(1), Art. no. 015201 (2010).
- [12] L. V. Asryan, N. V. Kryzhanovskaya, M. V. Maximov, et al., *Semicond. Sci. Technol.* **26**(5), 055025 (2011).
- [13] A. E. Zhukov, N. V. Kryzhanovskaya, F. I. Zubov, Y. M. Shernyakov, M. V. Maximov, E. S. Semenova, K. Yvind, and L. V. Asryan, *Appl. Phys. Lett.* **100**(2), 021107 (2012).
- [14] L. V. Asryan, N. V. Kryzhanovskaya, M. V. Maximov, et al., *J. Appl. Phys.* **114**(14), 143103 (2013).
- [15] F. I. Zubov, A. E. Zhukov, Yu. M. Shernyakov, M. V. Maximov, E. S. Semenova, and L. V. Asryan, *J. Phys. Conf. Ser.* **643**, 012042 (2015).
- [16] L. V. Asryan, *Semicond. Sci. Technol.* **30**(3), 035022 (2015).
- [17] L. V. Asryan, *Opt. Lett.* **42**(1), 97 (2017).

## Quantum plateaus in dynamical Hall conductivity

Zh. Gevorkian

Yerevan Physics Institute, Alikhanian Brothers St. 2, 0036 Yerevan, Armenia.

Institute of Radiophysics and Electronics, Ashtarak-2, 0203, Armenia

Dynamic Hall conductivity  $\sigma_H(\omega)$  of a 2D electron gas with impurities in the perpendicular magnetic field is analyzed. Plateau like behavior at low frequencies as well as at high frequencies provided complete filling of Landau levels is predicted. The broadening of a Landau level separates two frequency regions with different behaviour. Imaginary part of dynamic Hall conductivity reveals oscillations in the localized states region. Comparison with the experiment is carried out.

## **Compact transcapacitance model for short-channel FinFETs**

Ashkhen Yesayan

*Institute of Radiophysics and Electronics, Alikhanian Brothers str. 1, 0203 Ashtarak, Armenia*

A compact capacitance model is developed accounting for small-geometry effects in FinFETs. While decreasing the channel length, the transcapacitance model becomes very sensitive to all short channel effects, both in moderate and strong inversion regimes. In addition, for short channel devices, we need to take into account the inter-electrode capacitive coupling in the subthreshold regime, which is not significant for long channel devices. The capacitance model is developed based on compact charge based drain current model previously developed in [1], which further was extended to short channel DG FinFETs [2]. The quantum mechanical effects, which are very significant for thin Fins, are included in the model. The effect of mobility degradation on C-V characteristics is also demonstrated.

The model was validated with numerical simulations and a good accuracy of the model has been demonstrated in all operating regimes.

[1] J.-M. Sallese, F. Krummenacher, F. Prégaldiny, C. Lallement, A. Roy, C. Enz, A design oriented charge-based current model for symmetric DG MOSFET and its correlation with the EKV formalism, *Solid-State Electron.* 49 (3) (2005) 485–489.

[2] A Yesayan, F Prégaldiny, N Chevillon, C Lallement, JM Sallese, Physics-based compact model for ultra-scaled FinFETs, *Solid-State Electronics* 62 (1), 165-173

## On a validity criterion for the Born approximation

L. B. Hovakimian

*Institute of Radiophysics and Electronics of NAS RA, 0203 Ashtarak, Armenia*

The Born approximation (BA) method is of widespread use in studies of forward and inverse scattering problems in quantum mechanics [1] and cross-disciplinary fields [2, 3]. When a zero-momentum (ZM) particle (plane wave with de Broglie wavelength  $\lambda \rightarrow \infty$ ) is elastically scattered by a radially symmetric potential [ $U(\mathbf{r})=U(r)$ ] in three space dimensions, the BA is believed to be satisfactory under the following validity criterion [1],

$$\left| \int_0^{\infty} rU(r)dr \right| \ll \frac{\hbar^2}{2m}, \quad (1)$$

in which  $m$  is the mass of the particle. In this presentation, a procedure is proposed for examining the progenitor of (1) in continuous  $2+\alpha$  dimensions ( $0<\alpha<\infty$ ). Our analysis proceeds along heuristic lines and utilizes the  $\alpha$ -dependent transformation properties of the radial wave equation. We show explicitly that in the asymptotic limit  $\alpha \gg 1$  the BA method can work for ZM particles even in situations where the criterion (1) is violated.

[1] D. I. Blokhintsev. *Quantum Mechanics* (Springer, 2012).

[2] J. Li, X. Wang, and T. Wang. On the validity of Born approximation. *Prog. Electromagn. Res.* **107**, 219 (2010); D. Tajik, A. D. Pitcher, and N. K. Nikolova. Comparative study of the Rytov and Born approximations in quantitative microwave holography. *Prog. Electromagn. Res. B* **79**, 1 (2017).

[3] B. Krueger, T. Brenner, and A. Kienle. Solution of the inhomogeneous Maxwell's equations using a Born series. *Optics Express* **25**, 25165 (2017).

## Characterization of CZTS thin films synthesized by two-stage magnetron sputtering on Mo covered perlite glass-crystalline substrate

S. Petrosyan,<sup>1</sup>N. Yeranyan<sup>1</sup>, A. Musayelyan<sup>1</sup>, S. Pashayan<sup>2</sup>.

<sup>1</sup>*Institute of Radiophysics and Electronics NAS of Armenia, Alikhanian Brothers str. 1, 0203 Ashtarak, Armenia*

<sup>2</sup>*Institute for Physical Research NAS of Armenia, 0203, Ashtarak, Armenia*

In this research we present technology of two-stage synthesis of polycrystalline thin films based on the CZTSe kesterite material for the use in thin-film solar cells (SC). Initially, a thin layer of molybdenum (Mo) was deposited on special perlite glass-crystalline substrates by magnetron sputtering as the back contact of the SC. Next, by two-stage magnetron sputtering metal precursors Cu, Zn, Sn were formed to create a photoactive layer of SC, followed by selenization and annealing. The CdS buffer layer was deposited on the CZTSe films using electrochemical bath deposition method. Then, thin films of ZnO and ZnO:Al were deposited on the obtained structure by magnetron sputtering. Finally Ni/Al metal contacts were deposited by thermal sputtering technique.

The morphology of CZTSe thin films was studied using an atomic force microscopy (AFM). The thickness of the layers was measured with the Mitutoyo SurfTest SJ-410 profilometer, current-voltage measurements were carried out both without lighting and under standard 1.5AM lighting by Keithley-6340 unit at room temperature.

The thickness of the photoactive layer was about of 1-1.3  $\mu\text{m}$ . The conductivity of films is p-type, and the grains of a round shape with an average size of 700 nm. For the measured short circuit current density and open circuit voltage, correspondingly, 20  $\text{mA}/\text{cm}^2$  and 0.6V, the conversion efficiency of the SC was about 4.9%. This result is comparable with the available in the literature results for more efficient solar cells grown on glass substrates.

## Electrical characteristics of Sb-n-InSb Schottky barrier diodes

S.G. Petrosyan<sup>1,2</sup>, A. Khachatryan<sup>2</sup>

1 Russian-Armenian University, Armenia, 0051, Yerevan, Ovsepa Emina 123,

2 Institute of Radiophysics and Electronics NAS of Armenia, Armenia, 0203, Ashtarak, Br.

Alikhanyan Str. 1,

E-mail: [stepan.petrosyan@rau.am](mailto:stepan.petrosyan@rau.am)

Among the III-V binary semiconductor compounds, indium antimonide (InSb) has the smallest band gap (0.23 eV at 77 K), the highest mobility for electrons (more than  $10^6 \text{ cm}^2 \text{ V}^{-1} \text{ s}^{-1}$  in low doped material at 77K) and is widely used for manufacturing high speed photo-detectors in the middle IR range (3-5  $\mu\text{m}$ ) corresponding to one of the atmospheric transparency windows. Such photo-detectors have received wide applications in thermal imaging, detection and guidance systems. For Schottky contacts based on such a narrow-gap semiconductor as InSb, the presence of an interfacial layer and surface states is more critical, since the expected barrier height in the absence of an inversion layer is small, of the order of 0.1 eV. Therefore, to create a Schottky contact, it is necessary to choose a metal with a work function not very different from the work function of n-InSb, equal to about 4.6 eV for doping with  $10^{15} \text{ cm}^{-3}$  and an electron affinity of 4.59 eV [1]. Since according to the literature, Sb has a work function of  $\sim 4.5$  eV, we expected that its choice as a metallic electrode would yield a Sb-n-InSb Schottky diode, possessing not only good rectifying properties, but also a large photosensitivity in the middle IR range.

In the present work, the Schottky Sb-n-InSb contacts were fabricated by the method of laser pulse deposition, their current-voltage and capacitance-voltage characteristics were measured and analyzed. The photosensitivity spectra of fabricated Schottky photodiodes were also measured. To analyze the measured electrical characteristics, to compare with experiment, and to determine the parameters of the fabricated surface-barrier structures, theoretical expressions derived in the general model of a metal-semiconductor contact with a Schottky barrier will be used, taking into account the presence of a thin interfacial dielectric layer and surface states at the semiconductor-dielectric interface. The effective thickness of the dielectric gap and the density of surface states will be estimated.

## Charge transport mechanism in p-InSb/n-CdTe heterostructure

S. Petrosyan<sup>1,2</sup>, L. Matevosyan<sup>2</sup>, K. Avjyan<sup>2</sup>

<sup>1</sup> Russian-Armenian (Slavonic) University, Hovsep Emin str. 105, 0051 Yerevan, Armenia

<sup>2</sup> Institute of Radiophysics and Electronics, Alikhanian Brothers str. 1, 0203 Ashtarak, Armenia

Previously, p-InSb/n-CdTe hetero-structures (HS) for infrared (2-5.8 $\mu$ m) sensitive photo-detectors were fabricated by using of a simple low-temperature pulsed laser deposition technology (excluded the implantation, high-temperature diffusion and annealing processes) [1, 2]. Such heterostructure exhibits good rectifying characteristics at liquid nitrogen temperature (77 K). However, the mechanism of charge transport in p-InSb/n-CdTe HS has not been studied in detail until now.

Based on the measured at 77 K current-voltage characteristic of p-InSb/n-CdTe HS the study of charge transport through the heterostructure is presented. Fig. 1 shows the current-voltage characteristic of the structure built in a semi-logarithmic (fig. 1a) and a double-logarithmic scale (fig. 1b). It is established that the forward current is due to thermionic emission at a bias  $0.03 \div 0.17$  V and is described by usual exponential law with non ideality coefficient  $\eta=1$ , but for voltages exceeding 0.2 V the injection currents are observed to follow the law  $I \sim U^{3/2}$ . Taking into account the peculiarities of bands offset leading to the appearance of an inversion layers for electrons near the HS interface and therefore the existence of two reservoirs for electrons to supply the minority carries to the quasi neutral part of p-InSb a theoretical model is presented, which explains such current-voltage characteristic.

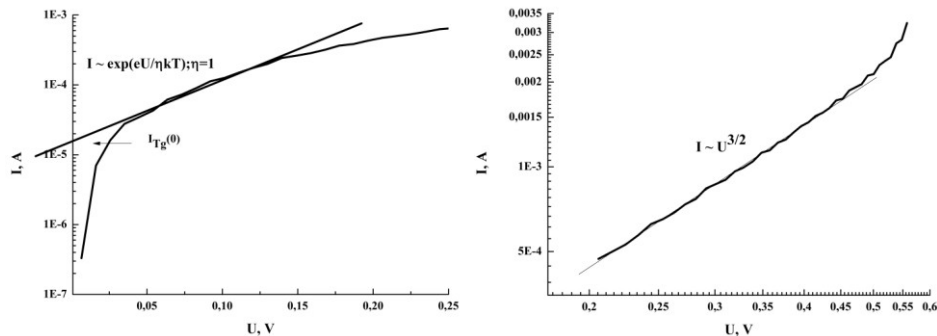


Fig. 1 The current-voltage characteristic of pInSb/nCdTe HS.

[1] Alexanian A.G., Aramyan N.S., Avjyan K.E., Khachatryan A.M., Grigoryan R.P. and Yeremyan A.S. Technology of PLD for photodetector materials. in: Combinatorial and High-Throughput Discovery and Optimization of Catalysts and Materials, edited by R.A. Potirailo and W.F. Maier, CRC/Taylor & Francis, 2006.

[2] L. A. Matevosyan, K. E. Avjyan, S. G. Petrosyan, A. V. Margaryan. "Photoelectrical properties of (p)InSb-(n)CdTe heterojunction". USPEKHI PRIKLADNOI FIZIKI (ADVANCES IN APPLIED PHYSICS) Vol. 2, No. 4, p. 403 (2014).

The work was carried out in the joint laboratory of the Russian-Armenian (Slavonic) University (RAU) and the Institute of Radiophysics and Electronics with the financial support of the RAU as part of the MES RF subsidy.

## Magnetic field control of phonon-mediated decoherence of spin-based qubit in two-dimensional quantum dot embedded in a suspended slab

Arshak L. Vartanian

*Department of Solid State Physics, Yerevan State University, 1. Al. Manoogian, Yerevan 0025, Armenia  
E-mail: vardan@ysu.am*

Quantum information and quantum computation implementation in terms of electron charges and spins have attracted tremendous attention for the development of large scale quantum information processing [1]. The electron-phonon interaction plays a very important role in ensuring spin coherence in QD structures. Suppression of this interaction leads to improvement of the quality of qubits. One way to solve this problem is the use of phonon confinement effect in semiconductor nanostructures. Control of the phonon density of states opens up the possibility of designing a spectrum of lattice vibrations and, in particular, suppression the electron-phonon interaction in low-dimensional systems. From this point of view the creation of quantum dot systems in suspended semiconductor slabs (so-called “phonon cavities”) is a significant achievement. In this regard, considerable progress has been made in the fabrication of nanostructures that are only partly suspended or even free-standing [2]. Such structures may be fabricated by various etching and lithographic techniques or by metal-organic epitaxy.

The spin relaxation caused by both spin-orbit and electron-acoustic phonon interactions in a two-dimensional quantum dot embedded in a free-standing semiconductor slab in the presence of a perpendicular magnetic field has been systematically investigated. Analytical expressions for the relaxation rate caused by the electron scattering on dilatational and flexural acoustical phonon modes have been obtained. The obtained results demonstrate the allowed and forbidden regions of spin relaxation rate as a function of magnetic field. The relaxation rate due to Dresselhaus term substantially exceeds the Rashba term ones. It has been shown that the relaxation rate, depending on magnetic field, can change in a very large region which can be used of provision for required rate by means of magnetic field. Also, by means of gate-voltage it is possible to realize the confinement, which makes the required transition rate between certain states available.

[1] R.B. Liu, W. Yao, and L.J. Sham, Quantum computing by optical control of electron spins. *Adv. Phys.* **59**, 703 (2010).

[2] R.H. Blick, M.L. Roukes, W. Wegscheider, and M. Bichler, Freely suspended two-dimensional electron gases. *Physica B* **249**, 784 (1998).

## The influence of the transverse electric field on the hot electron energy loss rate via polar-optical phonons in nanowires

A. Asatryan, A. Stepanyan, M. Yeranosyan, A. Kirakosyan, A. Vartanian

*Department of Solid State Physics, Yerevan State University, 1, Al. Manoogian, Yerevan, 0025, Armenia*

Among several optoelectronic devices, photodetectors which sense light signals by converting them into electrical signals have sparked great deal of interests because of their usages in imaging techniques as environmental monitoring, binary switch, optical communications, as well as implications in future photonic circuits. One-dimensional semiconductor nanostructures, particularly nanowires, are highly valued candidates for efficient photodetection with high responsivity, because of their large surface-to-volume ratio and direct charge transport pathway. Moreover, because of radial strain relaxation, nanowires are more amenable to bandgap engineering than planar devices [1] and their optical properties are highly tunable [2].

In the present work, we have investigated the hot-electron energy-relaxation processes in nanowire based photodetectors. Carriers in nanowire gain energy at a rate much faster than that for them to lose energy to the lattice, either by optical excitations or by a strong applied electric field. As a result, electron gas becomes “hot”; i.e., it goes out of equilibrium with the lattice attaining higher electron temperature than the ambient lattice temperature. As transport properties at high fields are determined by these hot carriers, the understanding of this hot carrier energy relaxation process is therefore of central importance in high-field carrier transport; furthermore, it is a crucial issue affecting the performance characteristics of ultrafast, high-field devices. We have calculated the hot-electron energy-relaxation rate in nanowires for intrasubband and intersubband scattering via interface optical- and confined LO-phonons in a perpendicular electric field. The hot-electron system has been described within the frame of the electron-temperature model. We have studied particularly, the dependences of average energy loss rate on the wire radius, electrical field strength, and electron temperature. It has been shown that the energy loss rate is more sensitive to the electric field applied perpendicularly to nanowire axis, when the wire radius is larger. Therefore the electric field can serve as a means to control the energy loss rate when electron-polar optical phonon interaction becomes dominant scattering mechanism.

- [1] C. Thelander, P. Agarwal, S. Brongersma, J. Eymery, L.F. Feiner, A. Forchel, M. Scheffler, W. Riess, B.J. Ohlsson, U. Gösele, L. Samuelson, *Mater. Today* **9**, 28–35 (2006).
- [2] L. Cao, J.S. White, J.-S. Park, J.A. Schuller, B.M. Clemens, M.L. Brongersma, *Nat. Mater.* **8** 643–647 (2009).

E-mail addresses: [annaa@ysu.am](mailto:annaa@ysu.am) (A. Asatryan), [astepanyan@ysu.am](mailto:astepanyan@ysu.am) (A. Stepanyan), [myeranos@ysu.am](mailto:myeranos@ysu.am) (M. Yeranosyan), [kirakosyan@ysu.am](mailto:kirakosyan@ysu.am) (A. Kirakosyan), [vardan@ysu.am](mailto:vardan@ysu.am) (A. Vartanian)

## Single-layer amorphous carbon anti-reflective coatings obtained by pulsed laser deposition method

L. Matevosyan<sup>1</sup>, G. Pluzyan<sup>1</sup>, K. Avjyan<sup>1</sup>, G. Dabaghyan<sup>2</sup>

<sup>1</sup> Institute of Radiophysics and Electronics, Alikhanian Brothers str. 1, 0203 Ashtarak, Armenia

<sup>2</sup> Institute of Information and Telecommunication Technologies and Electronics (National Polytechnic University of Armenia), Teryan str. 105, Yerevan, Armenia

The modern applications of amorphous carbon (a-C) and hydrogenated (a-C:H) diamond-like carbon (DLC) coatings are limited by industrial tribological applications. The use of such materials in functional electronics is strongly limited due to their high defect state density and successful applications are only in supplemental nature (e.g., biocompatibility, protective and anti-reflectivity).

Single-layer a-C anti-reflective coatings on the Si and GaAs substrates were obtained in this paper by using of a pulsed laser deposition (PLD) method. Based on the studies of optical reflection spectra, it is established that single-layer a-C coatings effectively reduce the high reflection of substrates (on average to 4 % for Si and 8 % for GaAs in 400-750 nm wave range) (fig. 1.). The reflection minimum (0.086%) on the Si substrate is observed at a wavelength  $\lambda_0 = 550$  nm (a-C film thickness - 75 nm). This value is 0.84% at a wavelength  $\lambda_0 = 522.7$  nm for a GaAs substrate coated with the same thickness of a-C film.

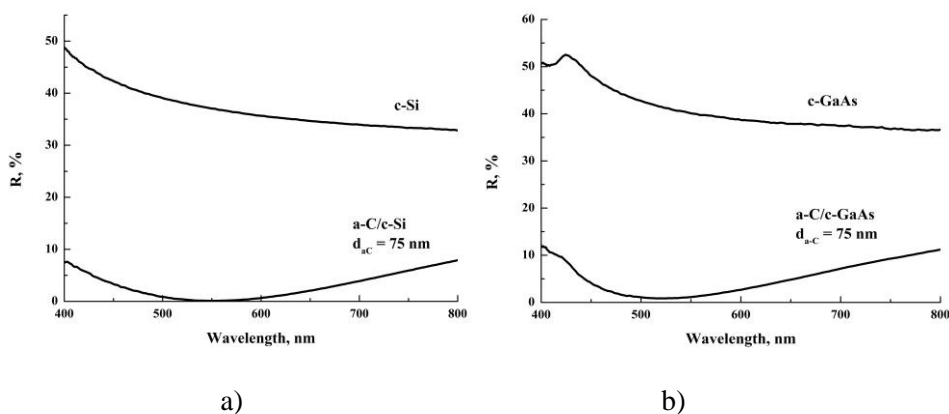


Fig. 1 Reflectance spectra for a) a-C/c-Si and b) a-C/c-GaAs structure (a-C film thickness - 75 nm).

Used by us PLD technology for fabrication of a-C anti-reflective coatings is very simple (excludes high-energy implantation, high-temperature diffusion and deposition processes) and applied for the first time.

**Wireless communications and related information  
technologies, (WL)**

**Session Chair:**

**Tigran Zakaryan, *IRPhE***

## **A Novel CoAP NB-IoT Testing Solution for 5G Wireless Networks Validation**

Prabhjot Bali, Hayk Manukyan, Evan Gray

*VIAMI Solutions, Longacres House, Six Hills Way, STEVENAGE, Herts, SG1 2AN, United Kingdom*

The 5G system can flexibly support a large variety of fundamentally different services. It is going to be one common network that can provide all generic services and flexible enough to change the service dynamically. It focuses on the three generic areas to cater most of the use cases: Enhanced Mobile Broadband (eMBB), critical Machine-Type Communications (uMTC) and massive Machine-Type Communications (mMTC). Enhanced Mobile Broadband (eMBB) provides both extreme high data-rate and low latency communications with extreme coverage. Critical Machine-Type Communications (uMTC) provide ultra-reliable low-latency communications for services with extreme requirements of availability, reliability, and latency and massive Machine-type communication (mMTC) is about providing wireless connectivity to millions of low-complexity and low-power machine-type devices transmitting a low volume of data.

This paper focuses on mMTC and its implementation using NarrowBand-IoT (NB-IoT). NB-IoT (or LTE Cat NB1) is a low-power wide-area network (LPWAN) radio technology standard developed to enable a wide range of devices and services to be connected using cellular telecommunication bands. It focusses on low-cost devices with lower-energy consumption and higher coverage requirements. NB-IoT requires very narrowband 200kHz (180 kHz plus guard-bands) for operation and can be deployed in three different operation modes - (1) stand-alone as a dedicated carrier, (2) in-band within the occupied bandwidth of a wideband LTE carrier, and (3) within the guard-band of an existing LTE carrier. In stand-alone deployment, NB-IoT can occupy one GSM channel (200 kHz) while for in-band and guard-band deployment, it will use one physical resource block (PRB) of LTE (180 kHz). Also, using a lightweight constrained application protocol (CoAP) over NB-IoT further demonstrates resource efficient solution.

This paper further discusses the use of lightweight constrained application protocol (CoAP) over cellular NB-IoT for data transfer. CoAP is designed for the needs of constrained devices. This protocol is built on top of UDP and provides data transfer security using Datagram Transport Layer Security (DTLS).

This paper finally discusses two optimizations for cellular IoT (CIoT) in Evolved packet system (EPS): User Plane CIoT EPS optimization and the Control Plane CIoT EPS optimization. With the User Plane CIoT EPS optimization, data is transferred in the same way as the conventional data traffic, i.e. over radio bearers via the SGW and the PGW to the application server whereas, in Control Plane CIoT EPS optimization, there is no data radio bearer set up, data packets are sent on the signaling radio bearer instead. Consequently, Control plane solution is most appropriate for the transmission of infrequent and small data packets.

VIAMI Solutions as a test equipment manufacturer has successfully demonstrated testing capabilities for CoAP based NB-IoT smart meters using their products TM500 and TeraVM (TVM). This solution has helped to test the capability and performance of the mobile network when flooded with massive amounts of connections and data. It can be scaled up without the cost and complexity of having to add additional hardware. VIAMI has implemented CP optimization where user data packets are encapsulated in Non-Access Stratum signaling messages towards MME (Data over NAS) resulting in a reduced number of control plane messages to send a short data transaction.

## Advanced modulation and coding challenges on the way to 400G and terabit Ethernet

D. Titov

*Keysight Technologies, Moscow, Russia*

The most common modulation scheme for 100GE today is NRZ modulation. 100GE is achieved by using 4 lanes of 25 gigabit per second (Gb/s) NRZ modulated signals. Theoretically, reaching 400GE speeds with NRZ is possible by applying these same concepts using 8 lanes of 56 Gb/s signaling. However, as speeds of NRZ designs increase above 28 Gb/s, channel loss of the transmission medium becomes a limiting factor. PAM4 signals use 4 amplitude levels with logical bits 00, 01, 10 and 11 to represent a symbol. The number of symbols transmitted per second (baud rate) is half the number of bits transmitted per second.

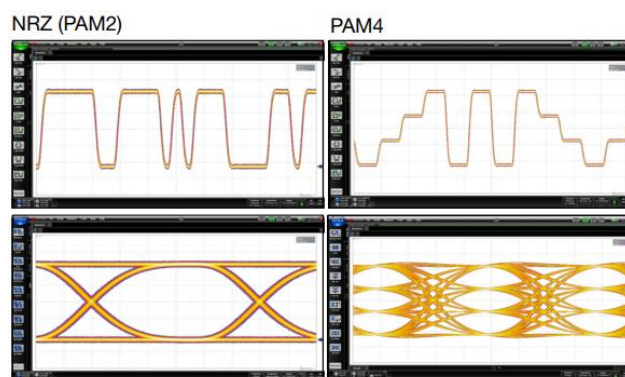


Fig. 1 NRZ vs PAM4 Modulated Signals

However, PAM4 designs are far more susceptible to noise since four signal levels are packed into an amplitude swing of two, as shown in Figure 1. Therefore, the signal to noise ratio (SNR) is lower, and analyzing noise from transceiver designs needs to account for channel return loss, as well as noise from the test instrumentation. PAM4 will use forward error correction (FEC) to account for this

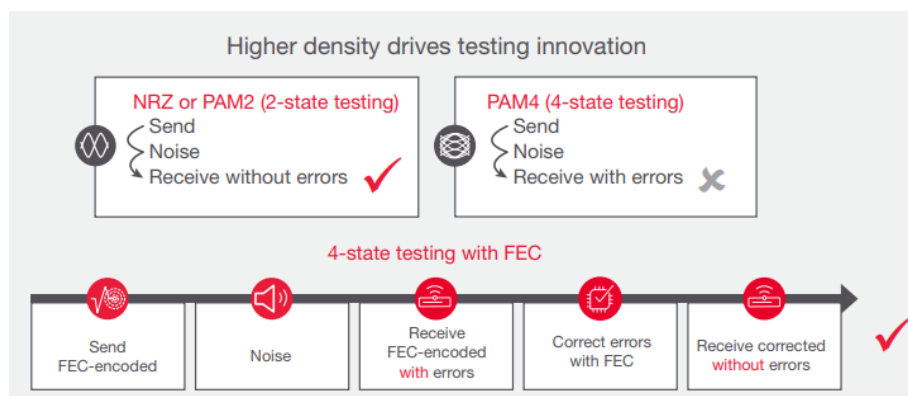


Fig. 2 Testing with and without FEC

**Keysight's newest state-of-art N4391B optical modulation analyzer** is designed for analysis of emerging perspective optical modulation formats. It supports transmission rates of 100/400 G and beyond up to 600G and 1T. With up to 110 GHz real-time bandwidth on all 4 channels N4391B makes it possible to dramatically increase the capabilities of the lab for testing high-speed signals with dual polarization and helps to reach the market first.

## Power Domain Non-orthogonal Multiple Access (PD-NOMA) technique for 5G networks

H. Haroyan<sup>1</sup>, G. Hovsepyan<sup>1</sup>, S. Sargsyan<sup>2</sup>.

<sup>1</sup> Yerevan State University, Alex Manoogian str. 1, 0025 Yerevan, Armenia

<sup>2</sup> Institute of Radiophysics and Electronics, Alikhanian Brothers str. 1, 0203 Ashtarak, Armenia

With the growing demands for high data rate, the use of millimeter-wave bands for next generation wireless communication network such as the fifth generation (5G) mobile systems attracts much attention of researchers. 5G promises a major change in mobility and, although not just 'built' for Internet of Things (IoT), it is heralded as a major driver of the growth of IoT [1].

Therefore, the existing OFDM technology may not be well suited for the transmission of the data of some 5G applications. Hence, several alternatives non-orthogonal multiple access (NOMA) have been proposed and will be considered for the 5G physical layer [2].

One of the most promising techniques is power domain non-orthogonal multiple access which takes advantage of users having different received power levels, either through power control or naturally occurring in the network, in order to separate the users. Power domain non-orthogonal multiple access (PD-NOMA) is used with successive interference cancellation (SIC) in order to cancel higher power signals, which are decoded first, before decoding the other users.

The idea is to allow at least one UE to be separated from the other UEs in the power domain at the receiver. This allows for the UEs to completely share the time and frequency resources.

One of the attractive features of PD-NOMA is that it can be used in combination with UL multiuser multi-input multi-output (MU-MIMO) schemes in order to further overload resources. This can be achieved in the uplink (UL) by using power control to have one UE transmit at a higher power level than the other UEs using the same resources. At the base station the UE with much higher received power is then decoded first by treating the other UEs as noise. After being decoded the user's signal is then canceled from the original received signal using SIC. The remaining users are then decoded. Fig. 1 shows a block diagram of PD-NOMA. The advantages of PD-

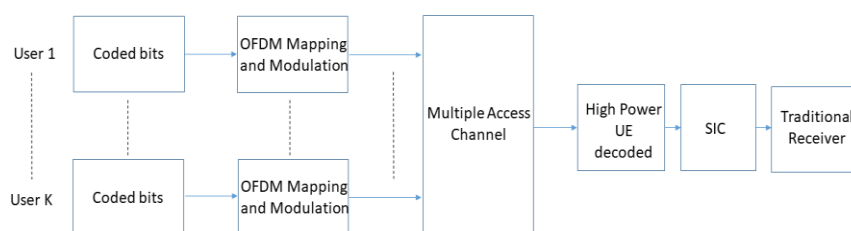


Fig. 1. Block diagram of PD-NOMA.

NOMA in the case of two users is demonstrated, there total system throughput is higher in comparison with traditional orthogonal multiplexing. Calculation method of channel budget and BER estimation for NOMA with proposed modulation scheme is developed. Orthogonal and non-orthogonal multiplexing methods

are compared from point of view BER. The possibility BER performance improvement for PD-NOMA in some scenarios is shown.

### References

- [1] Mattern, Friedemann; Floerkemeier, Christian. "From the Internet of Computers to the Internet of Things" (PDF). ETH Zurich. Retrieved 23 October 2016.
- [2] A. Benjebbour, Y. Saito, Y. Kishiyama, A. Li, A. Harada, and T. Nakamura, "Concept and Practical Considerations of Non-orthogonal Multiple Access (NOMA) for Future Radio Access", ISPACS 2013.

## OFDM Radar Signal Processing

G. Mkrtchyan<sup>1,2</sup>, A. Hakhumyan<sup>1</sup>, D. Nersisyan<sup>1,2</sup>, T. Manukyan<sup>1,2</sup>

<sup>1</sup>*Institute of Radiophysics and Electronics, Alikhanian Brothers str. 1, 0203 Ashtarak, Armenia*

<sup>2</sup>*YEA Engineering LLC, Engineering City, 21/1 Bagrevand str., Nor Nork, 0062 Yerevan, Armenia*

In General, the Orthogonal Frequency Division Multiplexing (OFDM) method was created for communication purposes as a digital Modulation technique, but nowadays it finds its own place in Radar applications.

OFDM method gives opportunity to generate not only OFDM signal, also generate all radar signals, which required. In other words, OFDM method is a universal method for creation radar signals

There are many investigations on using OFDM method in Radar application, such as: "Multi-frequency radar signals, Multi-frequency complementary phase-coded radar signal, OFDM signal constellation processing on Radar applications. Some work have been done for target detection and tracking, as well as direction of arrival estimation.

The research proves that the OFDM is ideal for both data transmission and radar sensing. The research have also been done in automotive radar applications and an OFDM joint radar and communication system have been created. Most of this research work defines the Doppler and range separately.

The method, suggested in this paper, can solve these tasks together within a single pulse.

Using the range-Doppler imaging algorithm with OFDM pulse radar, has been developed a system, which has an ability to create multi-target scenarios, test measurements results, as well as add noise, which didn't exist in the previous range-Doppler imaging algorithm. The Doppler frequency is estimated within one single pulse. It also has an ability add Gaussian White Noise, change The SNR for received signal, change the parameters for OFDM Radar and do all necessary measurements.

## **Novel Approach to Wireless Communications Software Development Performance and Productivity Evaluation – SAFe based**

Faris Muhammad and Charl Cilliers

*VIAVI Solutions*

This paper gives an overview of a method that can be used to evaluate the productivity of software/hardware development team. The approach is based on currently utilised Key Performance Indicator (KPI) in a product development programmes as part of VIAVI's R&D organisation. The method with all associated processes and their application are presented here. The outcome of the KPI is used to further improve the productivity of the teams and ensure adequate Return on Investment (ROI) as well as to initiate Root Cause Analysis (RCA) where necessary. This KPI enables devising performance benchmark for Individual Cross Functional Teams (XFT) and the overall Agile Release Train(s) (ART) where productivity can be monitored over any time granularity. Other secondary benefits of this KPI is to facilitate management decisions that include; which of the R&D site work assignment, where to scale up/down, what work allocation to which team, etc.

## Content-Aware Cross Layer Optimisation for IMT-Advanced Systems

M. S. Johal<sup>1</sup>, G. Markarian<sup>2</sup>

<sup>1</sup> Centre for Telecommunication Research and Innovation, Faculty of Electronics and Computer Engineering, Universiti Teknikal Malaysia Melaka, 76100 Durian Tunggal, Melaka, Malaysia

<sup>2</sup> School of Computing and Communications, InfoLab21, Lancaster University, Lancaster United Kingdom LA1 4WA

Radio Resource Management (RRM) is crucial to efficiently and correctly manage the delivery of quality-of-service (QoS) in IMT-Advanced systems. Various methods on radio resource management for LTE/LTE-Advanced traffic have been studied by researchers especially regarding QoS handling of video packet transmissions. Usually, cross-layer optimisation (CLO) involving the PHY and MAC layers, has been used to provide proper resource allocation and distribution to the entire system. Further initiatives to include the APP layer as part of CLO techniques have gained considerable attention by researchers. However, some of these methods did not adequately consider the level of compatibility of legacy systems and standards. Furthermore, the methods did not wholly address User Equipment (UE) mobility or performance metrics for a specific data type or a specified period.

Consequently, a content-aware RRM model employing a cross-layer optimiser focusing on a video conferencing/streaming application for a single LTE system has been proposed. Based on two constructed look-up tables, the cross-layer optimiser was found to dynamically adjust the transmitted video data rates depending on the UE or eNodeB SNR performance. The proposed look-up tables were derived from the performance study of the LTE classical (baseline) simulation model for various distances at a certain UE velocity. Two performance parameters, namely the average throughput and measured SNR were matched together to find the most suitable data rates for video delivery in both the uplink and downlink transmissions.

The developed content-aware RRM model was then tested against the LTE baseline simulation model, to benchmark its capability to be used as an alternative to existing RRM methods in the present LTE system. Based on the detailed simulations, the output performance demonstrated that for video packet delivery in both uplink and downlink transmissions, the content-aware RRM model vastly outperformed the legacy LTE baseline simulation model with regard to the packet loss ratio and average end-to-end delay for the same amount of throughput.

The baseline simulation model and the newly developed cross-layer approach were investigated and compared with practical measurement results in which PodNode [1] technology, besides other components and supporting simulation software, were used to emulate the LTE communication system. The first emulation experiment involving the baseline model was generally in sync with the uplink throughput simulation performance. The second test which implemented the cross-layer approach employing the look-up table derived from the previous emulated results, confirmed the viability of the proposed content-aware RRM model to be used in current LTE or LTE-Advanced systems for improving the performance in the packet loss ratio and average packet delay.

Reference:

- [1] Rinicom website. <http://www.rinicom.com/products/communications/podnode-i>

## Hybrid WiFi, WiMAX and LTE Network based on Quality of Service (QoS) using Opnet

Juwita Mohd Sultan<sup>1</sup>, Garik Markarian<sup>2</sup>, Dmitry Zvikhachevskiy<sup>3</sup>

<sup>1</sup>*CeTRI, Faculty of Electronic & Computer Engineering (FKEKK),  
Universiti Teknikal Malaysia Melaka (UTeM), Malaysia.*

<sup>2</sup>*Rinicom Ltd Secure Communications, Lancaster, Lancashire, United Kingdom.*

<sup>3</sup>*Huawei Technologies, London, United Kingdom.*

*juwita@utem.edu.my*

The guarantee of QoS allocation, especially in hybrid network is not easy because of the different mechanism in each broadband network. The differences for each wireless network can be stated as; Wireless fidelity (WiFi) could transfer data at a higher data rate with a lower cost, however limited to a certain size of area. The WiMAX signal could cover up to bigger scale in radius with high data rates as well, have a stable quality of service, with the advantage of seamless mobility between networks of different technologies, nevertheless the implementation is a bit costly. Meanwhile LTE data rate covers up to 300 Mbps in hundreds kilometers distance which reliably providing new future requirements for users.

Even though there are certain advantages for each network, self-reliant working mechanism of these networks produce a certain deficiency. In spite of obtaining the ultimate benefit from the current infrastructure, integrations of the network are a mandatory. However, this approach will not be profitable without developing and providing the QoS in the network classes implemented with the proposed network architecture. Since QoS assurance is critical in emergency disaster situation, therefore our focus is on hybrid WiFi, WiMAX and LTE benefited to the rescue team operations.

The propose architecture will evaluate using Opnet Modeler Simulation Tool and analyse the most important parameters in QoS; throughput, delay, packet loss. The aim of this project is to have an optimize throughput, zero delay and packet loss integrate with QoS allocation.